INFLUENCE OF PRE-ROLLING PROCESS ON THE MICROSTRUCTURE, MECHANICAL AND SHAPE MEMORY PROPERTIES OF CU-AL-NI SHAPE MEMORY ALLOYS

2022
MASTER THESIS
METALLURGICAL AND MATERIALS ENGINEERING

Mohammed Riyadh Abdulameer AL-MAHDI

Thesis Advisor
Prof. Dr. Hayrettin AHLATCI
Assoc. Prof. Dr. Safaa N.Saud Al HUMAIRI

INFLUENCE OF PRE-ROLLING PROCESS ON THE MICROSTRUCTURE, MECHANICAL AND SHAPE MEMORY PROPERTIES OF CU-AL-NI SHAPE MEMORY ALLOYS

Mohammed Riyadh Abdulameer AL-MAHDI

T.C.

Karabuk University

Institute of Graduate Programs

Department of Metallurgical and Materials Engineering

Prepared as

Master Thesis

Thesis Advisor
Prof. Dr. Hayrettin AHLATCI
Assoc. Prof. Dr. Safaa N.Saud Al HUMAIRI

KARABUK
November 2022

I certify that in my opinion the thesis submitted by Mohammed Riyadh Abdulameer AL-MAHDI "INFLUENCE OF PRE-ROLLING PROCESS ON THE MICROSTRUCTURE, MECHANICAL AND SHAPE MEMORY PROPERTIES OF CU-AL-NI SHAPE MEMORY ALLOYS" is fully adequate in scope and in quality as a thesis for the degree of Master of Science Metallurgical engineering

Prof. Dr. Hayrettin AHLATCI .....
Thesis Advisor, Department of Metallurgical And Materials Engineering

This thesis is accepted by the examining committee with a unanimous vote in the Department of Metallurgical and Materials Engineering as a Master of Science thesis. November 15, 2022

Examining Committee Members (Institutions)	Signature
Chairman : Prof. Dr. Mustafa ACARER (SU)	.....
Member : Prof. Dr. İsmail ESEN (KBU)	.....
Member : Assoc. Prof. Dr. Yunus TUREN (KBU)	.....
Member : Prof. Dr. Hayrettin AHLATCI (KBU)	.....
Member : Assoc. Prof. Dr. Safaa N.Saud Al HUMAIRI (MSU)	.....

The degree of Master of Science by the thesis submitted is approved by the Administrative Board of the Institute of Graduate Programs, Karabuk University.

Assoc. Prof. Dr. Müslüm KUZU .....
Director of the Institute of Graduate Programs

"I declare that all the information within this thesis has been gathered and presented in accordance with academic regulations and ethical principles and I have according to the requirements of these regulations and principles cited all those which do not originate in this work as well."

Mohammed Riyadh Abdulameer AL-MAHDI

ABSTRACT

M. Sc. Thesis

INFLUENCE OF PRE-ROLLING PROCESS ON THE MICROSTRUCTURE, MECHANICAL AND SHAPE MEMORY PROPERTIES OF CU-AL-NI SHAPE MEMORY ALLOYS

Mohammed Riyadh Abdulameer AL-MAHDI

Karabük University
Institute of Graduate Programs
The Department of Metallurgical and Materials Engineering

Thesis Advisor:
Prof. Dr. Hayrettin AHLATCI
Assoc. Prof. Dr. Safaa N. Saud Al HUMAIRI
November 2022, 80 pages

In the past years, vast advancements in science and technology have increased the demand for what is known as innovative or multifunctional materials. Thus, due to its potential high-temperature applications, Cu-Al-Ni shape memory alloys have recently attracted much interest.

This study attempts to investigate the different percentages of deformation of 1%, 2%, and 4%. on the microstructure, mechanical properties, and shape memory effect of Cu-13wt.% Al-4wt.% Ni shape memory alloys. The microstructures of the deformed and undeformed alloys were examined by optical (OM) and scanning electron microscopy (SEM). The phase analysis in terms of composition and classification was determined using X-ray diffraction (XRD). The phase transformation temperatures of the

deformed and undeformed alloys were identified by means of differential scanning calorimetry (DSC). The phase transformation characteristic of shape memory effect, hardness and stress-strain curves were found using tensile, hardness and recovery test, respectively. The findings indicated that the deformed specimen performed much better than the homogenized sample. From microstructural observations, it is seen that the β1′ (18R) and γ1′ (2H) martensite phases as needles- and plates-like morphologies coexisted at different fractions in the undeformed and deformed states.

Furthermore, the transformation temperature curves have shifted toward higher transformation temperatures as the deformation percentage increases. The deformed alloy exhibits good mechanical properties with high ultimate tensile strength and ductility after deformation at 2% and 4%, respectively. The microhardness of the deformed samples exhibited the lowest hardness of 247.6 Hv at a 4% deformation percentage. However, it exhibits ductile fracture, including mixed intergranular and transgranular features with linear stress-strain behaviour after applying a 4% deformation percentage. The shape recovery of 94.6 % of the original length was achieved when a 2 % of the deformation was applied. Because of this, it is reasonable to expect that the mechanical properties and shape-memory attributes of Cu-based SMAs are drastically affected by deformation.

Key Words : Cu-alloy, shape memory alloy, pre-rolling process, mechanical properties.

Science Code : 91515

ÖZET

Yüksek Lisans Tezi

INFLUENCE OF PRE-ROLLING PROCESS ON THE MICROSTRUCTURE, MECHANICAL AND SHAPE MEMORY PROPERTIES OF CU-AL-NI SHAPE MEMORY ALLOYS

Mohammed Riyadh Abdulameer AL-MAHDI

Karabük Üniversitesi
Lisansüstü Eğitim Enstitüsü
Metalurji ve Malzeme Mühendisliği Anabilim Dalı

Tez Danışmanı:
Prof. Dr. Hayrettin AHLATCI
Doç. Dr. Safaa N. Saud Al HUMAİRİ
Kasım 2022, 80 pages

Geçtiğimiz yıllarda, bilim ve teknolojideki büyük gelişmeler, yenilikçi veya çok işlevli malzemeler olarak bilinenlere olan talebi artırdı. Bu nedenle, potansiyel yüksek sıcaklık uygulamaları nedeniyle, Cu-Al-Ni şekil hafızalı alaşımlar son zamanlarda büyük ilgi görmüştür.

Bu çalışma, %1, %2 ve %4'lük farklı deformasyon yüzdelerini araştırmaya çalışmaktadır. Cu-13wt.%Al-4wt.%Ni şekil hafızalı alaşımların mikroyapısı, mekanik özellikleri ve şekil hafıza etkisi üzerine. Deforme olmuş ve deforme olmamış alaşımların mikro yapıları optik (OM) ve taramalı elektron mikroskobu (SEM) ile incelenmiştir. Bileşim ve sınıflandırma açısından faz analizi, X-ışını kırınımı (XRD) kullanılarak belirlendi. Deforme olmuş ve deforme olmamış alaşımların faz dönüşüm

sıcaklıkları, diferansiyel taramalı kalorimetri (DSC) vasıtasıyla belirlendi. Şekil hafıza etkisi, sertlik ve gerilim-gerinim eğrilerinin faz dönüşüm karakteristiği sırasıyla çekme, sertlik ve geri kazanım testi kullanılarak bulunmuştur. Bulgular, deforme olmuş numunenin homojenize edilmiş numuneden çok daha iyi performans gösterdiğini göstermiştir. Mikroyapısal gözlemlerden, β1′ (18R) ve γ1′ (2H) martensit fazlarının, iğne ve plaka benzeri morfolojiler olarak, deforme olmamış ve deforme olmuş durumlarda farklı fraksiyonlarda bir arada var olduğu görülmektedir.

Ayrıca, deformasyon yüzdesi arttıkça dönüşüm sıcaklığı eğrileri daha yüksek dönüşüm sıcaklıklarına doğru kaymıştır. Deforme olmuş alaşım, sırasıyla %2 ve %4'te deformasyondan sonra yüksek nihai çekme mukavemeti ve süneklik ile iyi mekanik özellikler sergiler. Deforme olmuş numunelerin mikrosertliği, %4 deformasyon yüzdesinde en düşük sertliği 247.6 Hv sergilemiştir. Bununla birlikte, % 4 deformasyon yüzdesi uygulandıktan sonra lineer stres-gerinme davranışı ile karışık taneler arası ve taneler arası özellikler dahil olmak üzere sünek kırılma sergiler. Deformasyonun %2'si uygulandığında, orijinal uzunluğun %94,6'sı oranında şekil geri kazanımı elde edildi. Bu nedenle, Cu bazlı SMA'ların mekanik özelliklerinin ve şekil hafızası niteliklerinin deformasyondan büyük ölçüde etkilenmesini beklemek mantıklıdır.

Anahtar Kelimeler : Cu-alaşım, şekil hafızalı alaşım, ön haddeleme işlemi, mekanik özellikler.

Bilim Kodu **:** 91515

ACKNOWLEDGMENT

At first and before everyone, I would like to thank God who helped me complete this study. Then I would like to express my thanks, appreciation, and respect to my family, especially my parents, who supported me morally and financially, without them, I wouldn't be where I am now. I would like to thank my friends who motivated me and helped me achieve this achievement. It is difficult to complete this thesis without the experience of my supervisor Prof. Dr. Hayrettin AHLATIC and Assoc. Dr. Safaa N.Saud Al HUMAIRI, whom I would like to thank for his support, assistance, and guidance to me, and I would like to thank the discussion committee for the long scientific time in studying this thesis and giving me some valuable advice and information.

In addition to, I would like to thank the KBU-BAP unit for supporting this study with BAP Project No: KBÜBAP-21-YL-101 by Karabuk University Scientific Research Projects Coordinator ship.

CONTENTS

Page

Page

Page

LIST OF FIGURES

Page

Page

LIST OF TABLES

Page

SYMBOLS AND ABBREVITIONS INDEX

SYMBOLS

α : Alpha Phase

β : Beta Phase

α' : the Hexagonal Martensite Phase

€i : Is the initial strain

€f : Is the final strain after heating

ABBREVITIONS

SEM Test : Scanning Electron Microscope Test

XRD Test : X-ray diffraction Test

DSC : Differential Scanning Calorimeter DSC7000 Series Test

EDX : Energy-dispersive X-ray spectroscopy

OM : Optical Microscopy

CHAPTER 1

INTRODUCTION

1.1. BACKGROUND OF THE STUDY

In the past years, the vast advancements in science and technology have increased the demand for what are known as smart or multifunctional materials [1]. These are lighter and stronger materials with unique properties that provide additional engineering functionalities. A subgroup of these multifunctional materials is the active materials, which exhibit sensing and actuation capabilities. Shape memory materials are a class of functional materials capable of converting a non-mechanical input, a thermal field, into a mechanical output, working as actuators [2, 3].

Within shape-memory materials, there is a category of materials called as have Shape Memory Alloys (SMAs), which have the ability to recover their original shape when the temperature is increased to a certain level [4, 5]. During the shape recovery, they are able to develop large forces, a fact that makes them exceptional actuators. Moreover, SMAs have superelastic behavior when activating at a specific temperature, and they are capable of recovering considerable deformations. In addition, SMAs have demonstrated energy dissipation capabilities, excellent corrosion resistance, hysteric damping, and good fatigue resistance [6, 7]. SMAs cover a wide range of applications in several industrial sectors and fields: biomedical, aerospace, automotive, oil exploitation, and structural [8, 9].

External non-mechanical inputs, such as magnetic or thermal fields, cause microstructural changes in the shape memory alloys (SMAs), which lead to their functions. SMAs that are thermally responsive are made up of two phases, each having its crystal structure and set of characteristics. These two phases are austenite (A), a high-temperature phase, and martensite, a low-temperature phase (M) [9,10]. The

crystal structure of austenite usually is cubic, but martensite might be tetragonal, orthorhombic, or monoclinic. It is reversible, solid-solid, and diffusionless because of the shear lattice deformation that causes the martensitic transition (movement of atoms from their original position). As the transformation takes place within a single crystal, it occurs along a particular lattice plane, known as the habit plane, which does not spin or deform during transformation. The martensitic transition can take place in two ways: via slip or by twinning. This second process happens most often in SMAs [11]. It involves atoms moving across a fraction of an atomic space, which causes relative atom displacement and a change in the shape of the SMA at a larger scale.

A variety of technological fields, including biomedicine [12] and a number of industries [13], have relied on Ti-Ni alloys (or Nitinol) for their exceptional success in the field of shape memory alloys. Nitinol, on the other hand, is more expensive than other alloys, and its transition temperatures (120 ^{o}C) are severely constrained. Shape memory alloys, which may be used as intelligent materials at high temperatures, are in high demand today (> 200 ^{o}C). Cu–Al–Ni alloys have been regarded as a better option for high-temperature applications than Nitinol. They have better thermal stability than titanium nickel, and their transition temperatures can reach as high as 240 ^{o}C [14, 15]; and they are also cheaper than titanium nickel.

Despite this, conventional cast polycrystalline Cu–Al–Ni alloys are extremely brittle [16, 17] due to their large grain size, solid elastic anisotropy, and significant orientation dependent transformation strain. Several events may occur even during the deformation of Cu-based SMAs, resulting in a macroscopic shape change. Plate versions that can accommodate themselves make up the thermoelastic martensitic structure. They merge and rearrange themselves during deformation to adapt to the shifting boundaries between different versions. During this process, mechanical twins can also be made.

The most favourably oriented martensite variants form as a result of the imposed stress. As a result of the deformation, martensite transformations, such as differences in the stacking sequence of densely packed planes and austenite martensite transformations, can occur as a result of the deformation [18, 19]. The deformation

mechanism in the martensitic state must be studied in order to understand the origins of the shape memory effect. In order to take advantage of SMAs' beneficial properties, it is also necessary to understand their tensile and compressive behaviour for specific applications. In recent years, the effects of martensitic deformation on SMAs have been extensively studied. Schroeder and Wayman [20] examined the microstructure of CuZn alloys caused by the production and displacement of martensite. Under stress, some SMAs have been demonstrated to display martensitic interface motion [21]. In a Cu-Zn-Al alloy, the substructure of martensite and the preceding interface structure in deformed martensite were investigated in great detail with the use of high-resolution electron microscopy [22]. Cu-Al-Ni SMAs have been extensively studied regarding martensitic transformation, mechanical and thermoelastic properties, and mechanical and thermoelastic properties under tensile pressures [23, 24]. As demonstrated in this study, Cu-Al-Ni SMAs were subjected to rolling deformation to establish the appropriate percentage of deformation, resulting in increased functional attributes.

1.2. PROBLEM STATEMENT

Various processing techniques and compositional modifications are employed to improve the mechanical properties of polycrystalline Cu-Al-Ni shape memory alloys. However, the development of SMA polycrystals' characteristics has lagged behind the researcher's aspirations for their use in engineering systems. As a result, SMA's mechanical properties are greatly affected by its temperature and the dominant phases involved. As a result, both an object's mechanical and functional aspects are inextricably linked. As a result, the stress required for detwinning or reorientation (dt) is less than the yield stress. Plastic deformation or plastic residual stresses are prevented, protecting the shape memory effect characteristics [25]. There is a strong link between a material's microstructure, mechanical properties, and thermomechanical factors like hysteresis and transformation temperatures. Excessive deformation may detriment the Cu-Al-Ni, which is brittle. Heat treatment or alloying components can be used to solve this issue. Cu-based shape memory alloys will be improved by using various pre-rolling deformation procedures to acquire the developed mechanical properties of Shape memory alloys. The microstructure of this new alloy is intended to improve its mechanical properties.

1.3. OBJECTIVES OF THE STUDY

The following are the objectives of this project:

1. To investigate the effect of the pre-rolling process on the microstructure characteristics of Cu-Al-Ni shape memory alloys.
2. To determine Cu-Al-Ni shape memory alloys' mechanical and shape memory behaviour after the deformation.

1.4. SCOPE OF THE STUDY

The following is an outline of the project's scopes:

1. Preparation of Cu-Al-Ni sample with the composition of $Cu_{100-x-y}$-Al_x-Ni_y (where x is 13 wt.% and y is 4 wt.%) using a tube furnace at a melting temperature of 1100 ^oC.
2. Differential scanning calorimetry DSC and Vicker's hardness tests were used to examine the as-cast samples for phase transition temperature and hardness measurements, respectively.
3. Perform the pre-rolling deformation process at 1 %, 2%, and 4% of different deformation percentages.
4. Analyses of the as-cast and deformed materials utilizing Optical Microscope (OM), Scanning Electron Microscopy (SEM), X-ray diffractograms (XRD), and energy dispersive spectroscopy (EDS).
5. Using an Instron 5982 universal testing equipment, conduct tensile tests on the as-cast and deformed samples to determine the fracture stress and strain.
6. Test the thermomechanical properties of the as-cast and deformed samples using an Instron 5982 universal testing equipment and then heat above the austenite finish temperature (A_f) to obtain the possible recovery.
7. Microstructure characterization of the fractured samples (fracture area) was examined using Scanning Electron Microscope (SEM).

1.5. SIGNIFICANCE OF THE STUDY

The importance of this research will be used to explain the fundamental mechanics which drive Cu-based form memory alloys (SMAs) deformation and failure and their possible improvement through the pre-rolling process. SMAs are classified as brutal to distinguish due to the complicated transitions in phases that create their distinctive features, including form memory. Those phase changes occur on several longitudinal scales (one of them being the macroscopic strain location twinning of martensite-austenite) and lead to a significant hysteresis. To begin, a mathematical understanding of this transformation behaviour is required in order to maximise the usage of this hysterical behaviour in energy storage and damping applications. A wide variety of solid-to-solid phase transformations and other strain localization mechanisms are suitable for the one-of-a-kind experimental approaches that have been established as part of the scope of this project. This is in addition to knowing how memory transition alloys work at their most basic level.

CHAPTER TWO

LITERATURE REVIEW

2.1. INTRODUCTION

As a result of their thermo-responsive characteristics, shape memory alloys (SMAs) have been considered alternatives to hydraulic actuators, pneumatic, and mechanical actuator-based systems. Shape memory effects (SME), pseudoelasticity, and thermoelasticity, all caused by the alloys' unique martensitic transformation properties, have led to the use of SMAs in various applications [26]. Pseudoelasticity, one-way shape memory effect (SME), and two-way shape memory effect (SME) are the significant impacts of SMAs generated by temperature or stress, depending on the loading route and the thermomechanical history of the material (TWSME). SMAs' transition temperatures are strongly influenced by their chemical makeup. When the constitution of a substance varies, so does the temperature at which it transforms. It is possible to adapt the material to achieve the required phase at the specified application temperature by adjusting the composition [27]. SMA alloy transition temperatures may be measured using a variety of methods. Electrical resistivity measurements and differential scanning calorimetric readings are the two techniques that are used the most often for the purpose of measuring the temperature of transitions. The term "shape memory alloys," or SME for short, may refer to a number of different types of alloys, including those based on NiTi, Cu, or Fe. Due to the significant strain recovery offered by NiTi in comparison to that of the other two potential materials, this alloy group has been the most economically feasible of the three alloy groups. However, because to the high processing and material costs associated with it, it has not seen widespread application in the commercial sector. Because of this, copper-based systems are the most viable option for applications requiring thermo-responsive shape memory over the long term from both an economic and a metallurgical point of view [28]. To put this another way, Cu-based alloy systems have lower production costs and

are more cost-effective than NiTi alloys due to the simplicity of processing the essential base metal (Cu) and the low cost of raw materials. Cu-base alloys are becoming formidable competitors for the majority of temperature sensing applications as a result of their moderate strain recovery ratio (5%), which is increased along with their electrical and thermal conductivity. Because of these additional advantages, copper based SMAs may have a greater chance of being economically viable for use in electrical and thermal actuator systems, such as circuit breakers, fire alarms, safety valves, louver openers, and heat engines. It has been shown that copper-based SMAs have a few drawbacks, including poor cold workability as a result of phase structures, grain size and sensitivity to martensite stabilization [9]. As a result of these issues, thermomechanical process, heat treatment and/or alloying modification can be addressed. Most Cu-based SMAs have struggled to deal with the phenomenon known as martensitic stabilization (sometimes referred to as martensite aging). Several researchers have explored and described the phenomenon. During repeated thermal cycling, a considerable shift in transformation temperature is noticed as its primary fingerprint, making it challenging to provide the consistent actuation response required within well-defined temperature ranges (which is critical for sensing applications). This aging effect is thought to be caused by a number of different processes. These mechanisms are two examples of pinning moving interfaces by flaws and martensite structural modification. Reordering (RO), short-range order (SRO), and long-range order (LRO) alterations of the martensite are the most common manifestations of the latter process. These methods considerably alter the austenite-martensite phase stability. According to previous research, the stability of martensite and austenite can be achieved by reducing their free energy due to changes in their symmetry and sub-lattice defects generated by diffusion. A material's martensitic condition causes the shape memory phenomenon, well-known to physicists (below M_f)[29]. In Cu-based SMAs, various deformation-related processes can result in a macroscopic shape shift. There are a variety of self-accommodating plate types in a thermoelastic martensitic structure. During the deformation, intervenient borders shift, coalescing and reorganizing these variations. Mechanical twins can form throughout this procedure. Applying pressure causes martensite to develop in an orientation that is preferable to stress. Another type of transformation that can occur in reaction to deformation is martensite transformation, involving changes in the stacking sequence of close-packed

surfaces; austenite transformations may also occur. It is not a new field, but research and development in Cu-based SMAs are showing promising results in improved transition temperatures, mechanical characteristics, fluid flow capabilities, and novel materials, as evidenced by a thorough literature study of the field[4]. In recent years, sensitive and cost-effective memory arrays (SMAs) have been synthesized, along with unique SMAs such as nanocrystalline, thin films, porous and/or amorphous structures that been developed with taken into consideration the feature of shape memory effect (SME) that made after an increase in temperature. A further calorimetric peak is observed due to this action, which delays the thermally induced transition to higher temperatures [30].

2.2. GENERAL SHAPE-MEMORY FEATURES OF ALLOYS

Due to their lower elements and manufacturing costs, Cu-based SMA is considered a possibility for other commonly produced SMA. They may be employed in high-temperature applications. Because of its brittle inter-granular fracture, polycrystalline Cu-based SMA is unsuitable for commercial use. Owing to the inconsistency of plastic and elastic deformations at grain boundaries and triple junctions, strong elastic anisotropy causes stress concentrations at grain boundaries and triple junctions [31, 32]. Polycrystalline Cu-based SMA has been subjected to a variety of processing methods as well as alloying elements for particle refining or precipitate generation, which has resulted in improved mechanical characteristics. Although polycrystal SMA characteristics have improved, the researchers' aspirations for their use in engineering systems have not been met, at least not yet. Because of the larger free surface area than the grain boundary areas, it is possible to develop single-crystal SMAs with good shape memory properties by using so-called oligocrystalline alloys. To protect the whole cross-section, the grains of these materials must be organized into a bamboo-like structure. As a result, they are restricted in terms of processing and application. SMAs also have issues with the stabilization of martensitic-austenite phases. Shape memory properties, such as stresses, temperature transformation, strain recovery, and features of hysteresis experienced during shape recovery, are affected by the change in temperature [33]. Because of thermal activation, phases can be stabilized at room temperature as well as at elevated temperatures. Alloy microstructure is closely linked

to the processing history of the material and its unique composition, as is intergranular fracture and phase stability (such as variants, defects, grain size, related phases, and types of martensitic phase) [34].

2.2.1. Shape Memory Effect Property

SMAs have the ability to undergo thermo-elastic martensitic transformation because of the shape memory effect (SME). The martensitic phase of the SMA will deform during loading and unloading at temperatures below M_f, resulting in a shape memory effect. Because of this, the original shape of these deformed alloys may be restored by heating them to temperatures above A_f. An example loading route 1 →2→3→4→1 is shown in **Figure 2.1**, where the SME characteristic may be noticed [35], as shown in the (1→2) cycle. When the parent phase is cooled, it changes into the twinned martensite. When the materials are subjected to stress (2 → 3), detwinning and inelastic strains can result. Unloaded, the martensite phase remains in the same state as the detwinned structure, with no recoverable inelastic stresses. After heating above A_f (4→1), the inelastic stresses are recovered, and the materials are restored to their original shape [35].

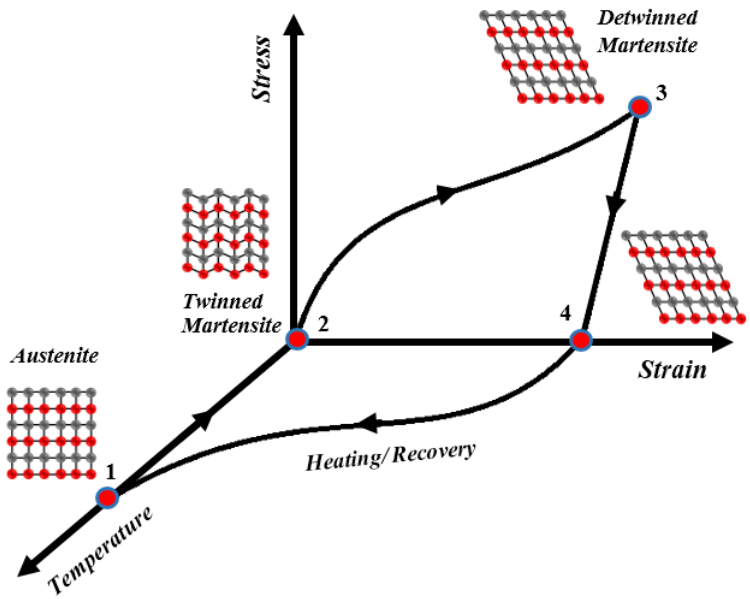

Figure 2.1. A diagram showing the relationships between strain, stress, and temperature for crystallographic changes during shape memory effect phenomena [35].

Martensitic variations (1→2) form during stress-free cooling in the austenite phase [36-38]. It is the self-accommodating structure that defines these alloys' crystallographic structures. Regarding SMAs, 24 varieties of martensite are divided into six self-adjusted categories <011> arranged throughout austenite poles with a typical diamond-like morphology in Cu-based alloys. These groups have no macroscopically observable strain, yet some martensite variations and twinning interface borders demonstrate extremely significant motions. Reorientation of variations occurs at temperatures lower than M_f, although the boundary junctions and detwinning morphology are performed at a lower stress value than that of the yield limit within the martensite plastic region. A considerable amount of inelastic strain will be produced in the second stage (2→3), and this strain will not be recovered when the load is removed (3→4) from the material. In the last stage (4→1), the inelastic strain is recovered by heating the deformed alloys to a temperature above A_f [35, 39, 40]. The martensitic phase change becomes unstable when the austenite completion temperature (A_f) approaches without external stress. Therefore, the reorientations of martensite variants take place; nevertheless, an additional strain will result in an inelastic strain degree, though in the opposite direction; consequently, the original shape will be recovered. Using a specially designed machine, such as the one shown in Figure 2, Saud et al. [41] partially recovered the shape of the part and then subjected it to additional heating > Af, which is 300 ^oC, which resulted in a complete recovery of the shape of the part. This was done using an external maffle furnace, as depicted in **Figure 2.2**, where the shape was fully recovered. As a result, the thermoelastic transition of Cu-based SMA is nearly complete. The basic features that promote their reversibility during the shift from austenite are their low hysteresis, limited volume change, and lack of plastic accommodation (also called the "parent phase") [42]. Due to this self-accommodation process, no macroscopic shape change is observable in the martensitic microstructure, which is generated by elastically accommodating the various variations (orientations of martensites) within a single favored variant. Loading can quickly alter this microstructure. Due to the fact that it may be reversed when subjected to heating in the austenitic region, the process results in a microstructure that has very few dislocations, if any at all [22].

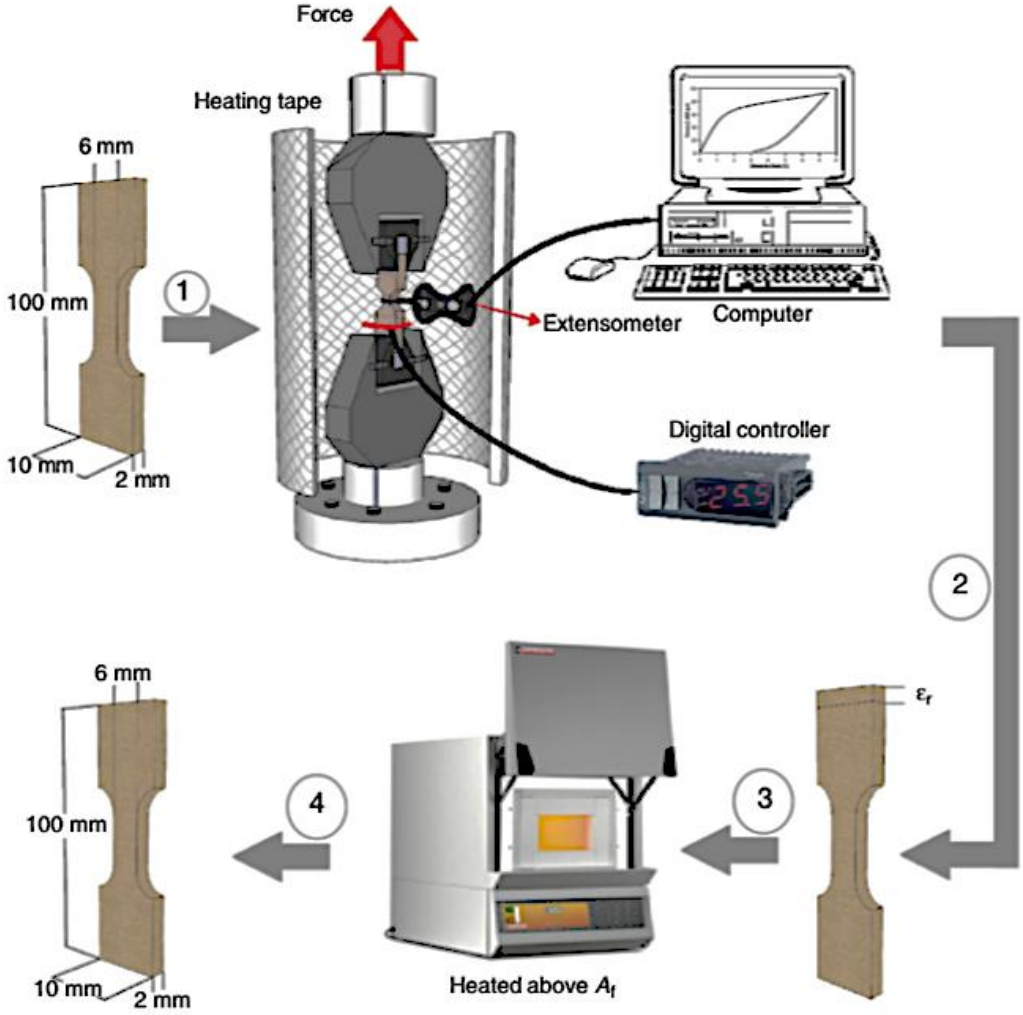

Figure 2.2. Test mechanisms for the Shape Memory Effect (SME) [41].

2.2.2. Pseudoelasticity Property

Pseudoelasticity is a property of shape-memory alloys that has a lot to do with how the induced strain recovers when the material is unloaded at temperatures above A_f. Generally, pseudoelastic loading directions begin in the austenitic area at zero stress, travel toward the detwinned martensite region, and then return to the starting position. Starting at point a in **Figure 2.3**, the flow of loading and unloading was depicted in the following order: b → c → d → e. Figure 2.3 is a schematic depiction of isothermal and isobaric loading routes.

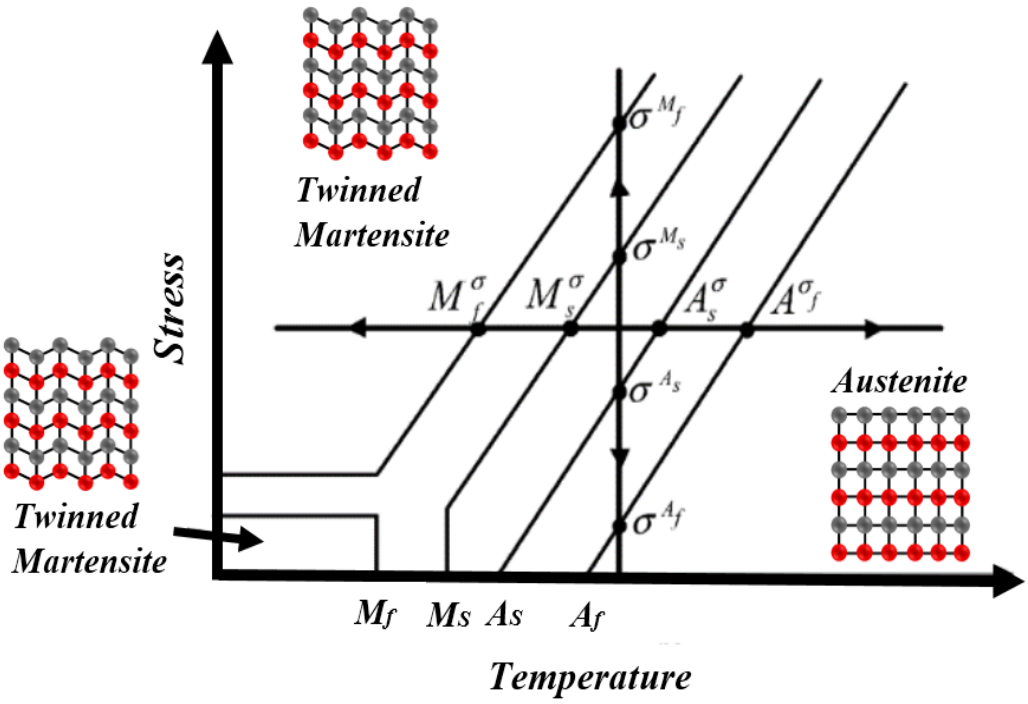

Figure 2.3. In pseudoelasticity in single-crystalline SMA, there are two loading routes to shape memory alloys [35].

The vast majority of shape memory alloys may be classified into one of these three primary categories within the alloys that exhibit both SME and superelasticity: copper-based SMA, nickel-titanium-based SMA, and iron-based SMA. Because of their superior functional qualities, the first two categories are more typically employed in engineering applications than the latter. It has been employed in the military, medical, safety, and robotics applications. NiTi alloys are used in aircraft components in the military sector. As tweezers, they are utilized to extract things via minor wounds; as a hook, they are employed in shoulder surgery; orthodontic wires, eyeglass frames, and catheter guides are examples of their medical use. Safety applications use a wide variety of sensors, including anti-scorching devices, sprinklers against fire, and other sorts of sensors. The mechanical energy derived from shape changes will be used in future electric generators, vehicle engines, aviation engines, and carburetor and engine lubrication controls. The exceptional shape memory of NiTi SMA makes it appropriate for a broad variety of applications, ranging from those in the medical field to those in the aerospace industry. Because of the significant expense of the alloying elements and also the considerable susceptibility of these SMAs to oxygen at increased

temperatures, the production of these SMAs is much more costly than that of copper based SMA. This results in an increase in the cost of the alloying elements [43].

On the other hand, Cu-based SMA is cheaper and thought to be better at transferring heat and electricity. SMAs based on copper have the highest thermal stability against aging and stabilization, making them the most desirable. Because of intergranular fracture, the deformation recovery and brittleness of Cu-based SMA at room temperature are less than ideal. When large grains are present, elastic and plastic inconsistencies between surrounding grains can lead to stress accumulation at the grain boundary, leading to grain boundary cracking. With thermomechanical processing, the grain size of Cu-based SMA was reduced to 5 m. This led to high fracture stress of 1200 MPa in tension and ductility of 10% in tension. In Cu-based SMA, Al may be replaced by Mn to enhance ductility and regulate grain size without substantially affecting the transformation temperature. This can be done in order to manage grain size and boost ductility. Grain size is decreased in Cu–Al–Ni systems as a consequence of the inclusion of low amounts of Ti, which has a limiting impact on grain formation, and the generation of Ti-rich nanosized precipitates during solidification also contributes to the reduction in grain size. For Zr and Si, for instance, both have the ability to decrease grain size. The mechanical features of these hybrid materials, copper-based alloys, have shown potential for future applications. It demonstrates tensile and deformation of fracture at roughly 830 MPa and 8% [44] in the Cu-13.4 wt.%Al-3.1wt.%Ni-0.06wt.%Si-0.58wt.%Zr SMA [45]. There is high fracture stress of 903 MPa and a significant amount of fracture deformation of 8.6% in tension in Cu-13.4wt.%Al-3.05wt.%Ni-0.24wt.%Ti-0.63wt.%Zr SM alloys. However, other Cu-based SMA systems, like the Cu–Al–Mn system, have shown better ductility.

2.3. COPPER SHAPE MEMORY ALLOY BASED TYPES

The binary system of the alloys such as Copper-Zinc (Cu–Zn) and/or Copper-Aluminum (Cu–Al) are the two primary classifications of shape memory alloys (SMAs) that are copper-based. There are many different applications for this third element alteration, therefore it may be used in either binary or ternary systems, depending on the demands of the end user, such as temperatures ranging from 100 ºC

to 370 ^{o}C. Both systems carry out their shape memory characteristics inside the domain of existence phases. From this vantage point, it was proved that transition temperatures are susceptible to the content of alloys. In order to attain repeatability that is more desired than 5^{o}C, it is often necessary to have an accuracy of 10^{-3} to 10^{-4} percent. Hysteresis is typically seen to be significantly lower in copper-based alloys in comparison to NiTi alloys. The copper, zinc, and aluminum alloy are not difficult to make and is quite affordable. When heated to a high enough temperature, it breaks down into the equilibrium phases, resulting in the martensite being more stable. To produce grains ranging in size from 50 to 100 nm, the availability of additives such as cobalt, zirconium, titanium, or boron is necessary. Boron can also be added to the material to increase its ductility, which is desirable. The Cu–Al–Ni system is noticeably less susceptible to problems associated with both stabilization and aging. This alloy operates with more negligible hysteresis than NiTi and becomes brittle when the nickel percentage is increased beyond 4 at. %. In addition, it is common practice to keep the percentage of nickel in the alloy at a fixed 4 at. %; the composition of this alloy is Cu96-xAlxNi4.

The martensite phase stability may be improved by increasing the amount of Al in the produced alloy. Adding Al is done to lower the temperatures required for the transformation. This variety has an almost entirely linear distribution, with values for M_f of 203 K and A_f of 250 K corresponding to a 14.4 at. percent Al and M_f of 308 K and A_f of 348 K corresponding to a 13.6 at.% Al [46]. As a result of the fact that temperatures are often operated across a broad range, the realistic upper limit for transformation is set at 473 K. When the temperature is raised over this point, there is almost likely going to be an abrupt decline in the transformation due to the effects of aging. The standard copper-based SMAs have the capacity to display a pseudoelastic strain of between four and six percent [47, 48].

Extremely high levels of pseudoelastic strain characterize the change from martensite to martensite. It is feasible to see approximately 18 % of the pseudoelastic strain adhere with a full recovery in a single crystal of $Cu_{81.8}Al_{14}Ni_{4.2}$ shape memory alloys [49]. The Cu-Zn alloy containing Sn as a 3rd element at a weight percentage of 34.7% has showed unusually low transition temperatures, with an Mf of roughly 208 K and an

Af of around 235 K. This might be explained by the fact that the Mf has a much lower temperature than the Af. Furthermore, this modification has shown a transition strain (εt) with a strain of 2.5 percent during all a pseudoelastic strain of 8 percent by achieving a complete strain recovery [50]. Recently, the binary alloy consisting of copper and aluminum has had a trace quantity (about 0.6 wt.%) of beryllium added to it as a ternary element. It was determined that adding this component caused a drop in the transition temperatures from 200 degrees Celsius to 150 degrees Celsius while maintaining a very high thermal stability level. Cu-based SMAs are made up of many various types of alloys; however, the Cu–Zn–Al and Cu–Al–Ni alloys, which have cheap production costs and great resistance to functional degradation as a result of treatment of aging, are the most often used alloys. Compared to other shape memory alloys, Cu-Al-Ni SMA is distinguished by a number of qualities, including a price that is significantly lower than that of Ni-Ti alloys and transformation temperatures that are significantly higher.

2.3.1. Cu-Al-Ni SMAs

Figure 2.4 depicts the vertical cross-section of the Cu–Al–Ni phase diagram when the Ni content is set to 3 wt.%. Only in the event that the martensitic transition has place would the alloy be able to display its shape memory capabilities. It is impossible to avoid a heat treatment since it is required to provide the undercooling essential for the martensitic transformation. It is performed by first annealing the material in the temperature range of the stable β phase and then immediately quenching it in water to get the desired structure (β quenching) [51].

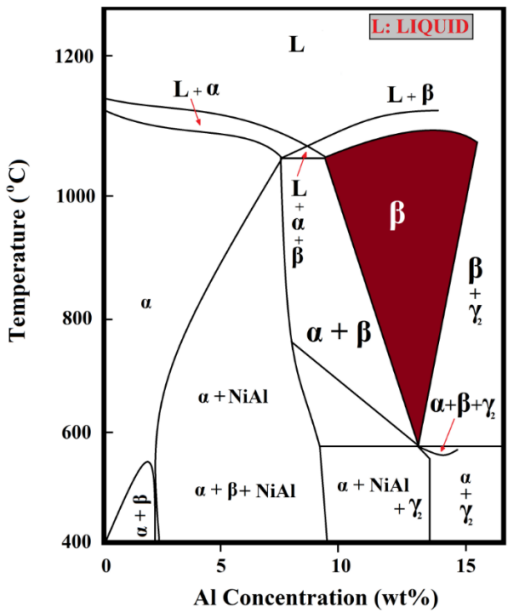

Figure 2.4. Diagram of the ternary phases Cu–Al–Ni as a vertical cross-section at a weight percentage of 3 wt. % of the Nickel element [52].

The martensitic transition can be caused either by heating the material to a high enough temperature or subjecting it to external stress. To put it another way, the change from austenite to martensite is driven by both the application of stress and a decrease in temperature. The Clausius–Clapeyron connection is a significant correlation between the two forces. This connection, which is generated from the thermodynamics correlations of the phase transition, is termed after the two researchers who were responsible for its discovery. Thermal treatments significantly impact the martensitic transformation's characteristics [53]. These characteristics include the martensite feature of hysteresis and phase transformation temperatures (A_s, A_f, M_s, and M_f) are significantly correspondent to the change of the phase order degree and formation and volume fraction of the precipitations/intermetallic compounds [54, 55]. Because of being cooled, the Cu-based SMAs go through a martensitic transition, which changes their structure from the Beta-phase to a close-packed structure and this occurs as a result of a change in their crystal structure.

Furthermore, the disordered BCC structure of the high-temperature phases in the Cu–Al–Ni SM alloys is a more stable formation compared with Cu–Zn–Al SM alloys [56]. Both $\beta`_1$ and $\gamma`_1$ forms of thermally induced martensites can occur in Cu–Al–Ni alloys. The formation of these martensite phases depends on the alloy's composition and the

heat treatment [57-60]. When the temperature drops, the a-phase loses some of its stability. For instance, the martensite phase can continue to be metastable even at lower temperatures if it is cooled appropriately (by air cooling) [61-63]. It is required to identify the stability limit of the overcooled martensite phase in order to avoid the expansion of the ordination state of the Beta-phase and/or the precipitation of the stable phases. Both of these outcomes would be undesirable. On the other hand, the production of alloys with a small grain size is intricately tied to the enhancement of the mechanical properties of Cu-Al-Ni SMA [64]. It is vital to identify the stability limit of the overcooled martensite phase in order to avoid the expansion of the ordination state of the Beta-phase and/or the precipitation of the stable phases. Both of these outcomes might be disastrous. On the other hand, the production of alloys with a small grain size is strongly associated to the enhancement of the mechanical properties of Cu-Al-Ni SMA [65, 66]. Compared with the reverse transformation, the martensitic transformation has a more considerable energy need [67].

Grain refiners are often included in the composition of Cu-Al-Ni shape memory alloys, which is done for a variety of reasons. These impacts might be classified as either direct or indirect, for example [68]; when intermetallic is formed, transformation temperatures are affected. This is due to a combination of factors, including the production of solid solutions, which can increase phase hardness, and grain expansion during the annealing process, which affects the transformation temperatures. The eutectoid response was stifled when Itsumi et al. [69] substituted 2% of the aluminum concentration for manganese, which had the opposite effect. $\beta_1 \rightarrow \alpha + \gamma_2$. This allowed for a reduction in brittleness, one of the most critical defects of Cu-Al-Ni SMAs; however, adding manganese did not lower the temperature at which the material transformed. They also employed 1% of the Ti, which led to grain refining and made it possible to do away with intergranular cracking. Karagoz and Canbay [70] researched how the phase transformation temps were affected by varying amounts of aluminum and nickel. They discovered that either forward or reverse transformation temperatures have significantly been impacted by the change of the Al weight percent. Consequently, more significant percentages of Al displayed lower transformation temperatures than lower percentages of Al produced. It was discovered that the change in the weight percent of Ni was primarily responsible for lowering the diffusivity of

both Cu and Al. As can be seen in **Figure 2.5(a-c)**, Chang [71] discovered that increasing the amount of aluminum from x= 13.0 to 14.5 resulted in a considerable reduction in the Ms temperature of Cu–xAl–4Ni SMAs, which went from 180.9 ^{o}C to -54.7 ^{o}C. This lends credence to the findings of the study that was carried out by Recarte [72]. He discovered that the temperature (Ms) of Cu–Al–Ni SMA was strongly part of the chemical composition of the material, particularly the quantity of Al that was present. This discovery lends support to the conclusion of the study. The shape memory alloys of Cu–xAl–4Ni with better absorption of aluminum brandishing a relatively low martensite start temperature might be since it's a fact perhaps the key driver requisite for martensite $\gamma`_1$ (2H) nucleation is significantly greater than the $\beta`_1$ martensite phase. In other words, the driving force required for nucleation of the $\gamma`1$ (2H) martensite is higher than $\beta`_1$ (18R) [72-74].

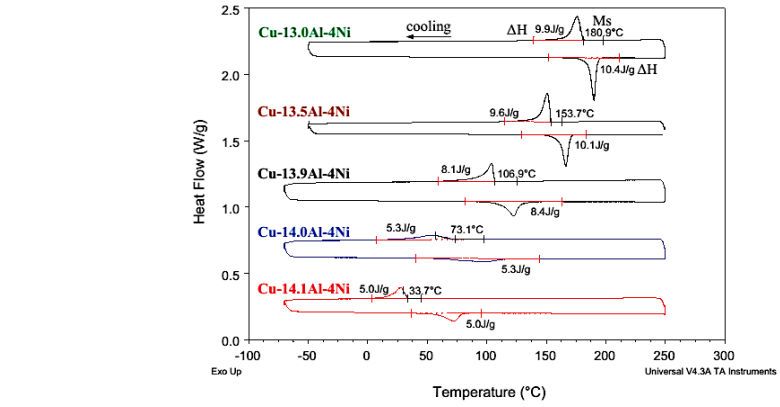

(a)

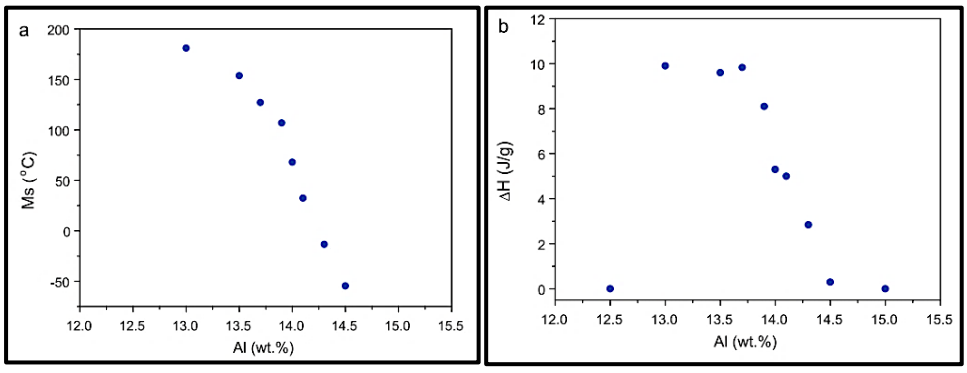

(b) (c)

Figure 2.5. The characteristics of transformation temperatures are (a) Heating and cooling curves, the effect of weight percentage of Al on the (b) martensite transformation temperature, and (c) enthalpy of the transformation [71].

Sampath [68] discovered that the addition of alloying elements and grain refiners are the primary variables that can improve the strength of a solid solution. This is because some of these components are able to dissolve into the solution, which results in the development of a second phase. As a result, the transformation temperatures are caused to rise when a trace quantity of Ti, Zr, and B is added to the Cu-Al-Ni SMAs, as demonstrated in Figure 2.6 (a-d). On the other hand, a rise in the transition temperatures was seen in response to a drop in the weight % of Al and Ni. Therefore, the transformation temperatures increase when there is less than 12 weight percent of Al, which is in exact accord with the findings of other studies [47]. From the same perspective as before, Miyazaki [16] discovered that the transition temperatures tend to drop when there is an rise in the quantity of aluminum and nickel in the overall of Cu-Al-Ni shape memory alloys composition. According to the findings of Sugimoto [75], the temperature of the transformation rises when varying amounts of titanium are mixed in with the copper, aluminum, and nickel in the SMA. These upturns are associated with the integration of the X-phase through into microstructure in the appearance of Ti-rich particles. This incorporation has the ability to limit the motion of interfaces across martensite and other phases, if formed. According to Lee et al. [76], the temperature at which martensite transforms behaves differently depending on the alloying element. As reported by these researchers, the temperature drops when there is an increase in the amount of Ti, but it rises when there is an increase in the amount of Zr. This can be explained by the dissolved titanium and zirconium proportion in the β-phase. J. Dutkiewicz and colleagues [45] disagreed with the statement that the addition of Ti reduced the Ms. Because the M_s temperature increases with decreasing grain size, they have shown that the temperature of transformation lowers more rapidly at smaller grain sizes. The existence of different kinds of precipitates that limited the consistency of the phase of the different temperatures and consequently resulted in the development of quality corresponding to 232 degrees Celsius, the observed peak's behavior is likely to be intense and board at 232 degrees Celsius and 350 degrees Celsius, respectively. In Figure 2.7 (a-d), Saud et al. [77] found that the temperature dependence of Cu-Al-Ni SMAs with Sn added was illustrated by the curves of exothermic and endothermic..

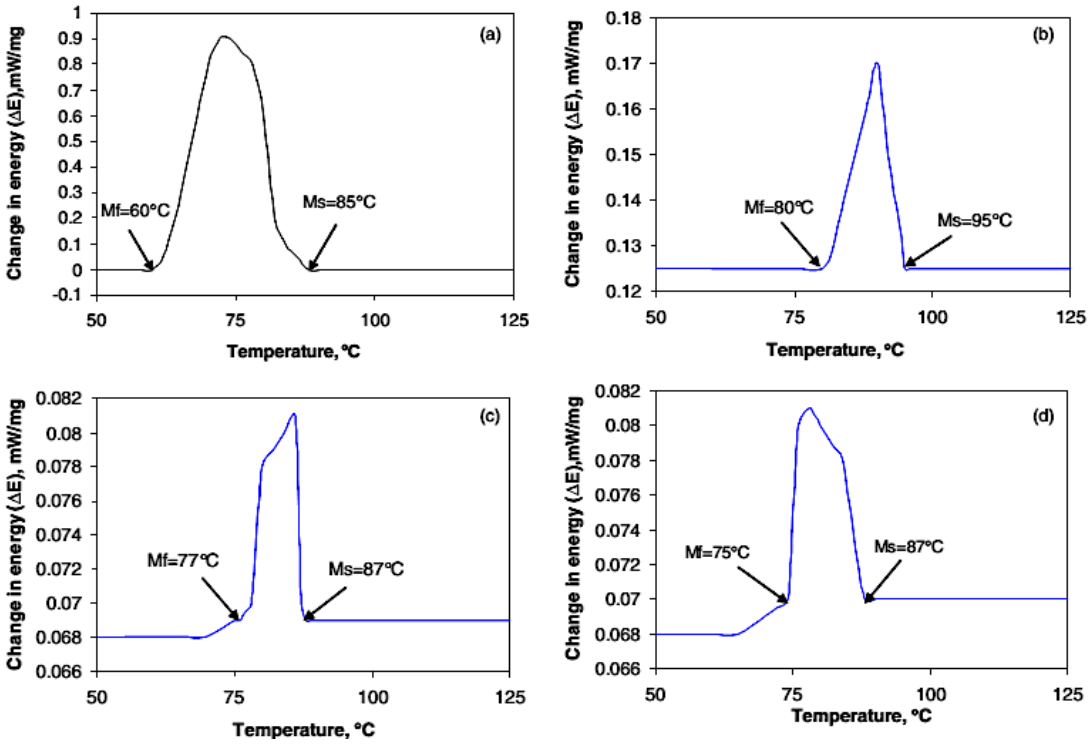

Figure 2.6. Profile curve of the DSC for the (a) Cu–Al–Ni; (b) Cu–Al–Ni–0.2Ti; (c) Cu–Al–Ni–0.4Mn;(d) Cu–Al–Ni–0.2Zr [68].

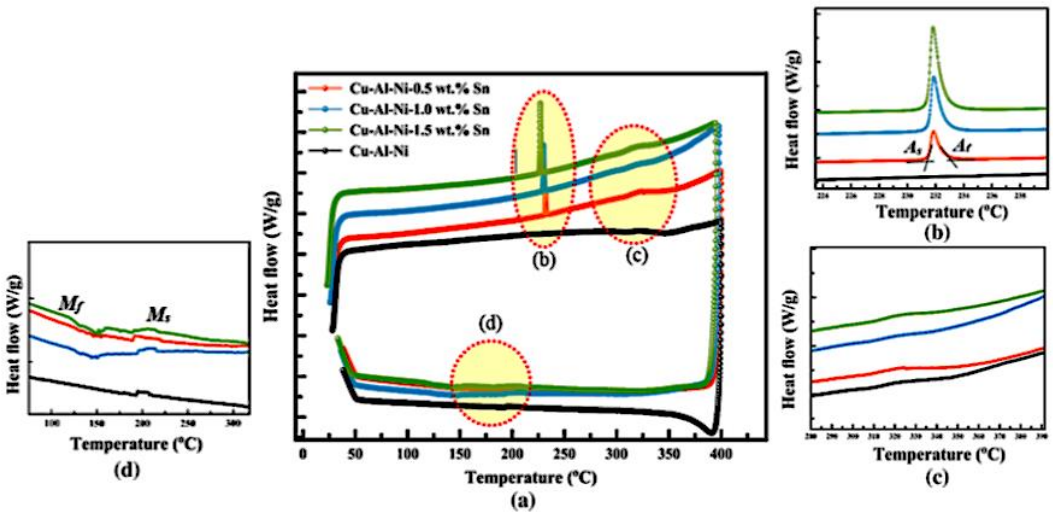

Figure 2.7. The heating and cooling curves of Cu-Al-Ni SMAs as a result of Sn addition, (a, b) forward transformation peaks, and (c) backward transformation peaks [77].

The needle and/or plate-like martensite morphologies can be generated in the microstructure of Cu-Al-Ni SMA [68]. Acicular morphology ($\beta`_1$ phase) and self-accommodating morphology ($\gamma`_1$) are two distinct phases that may be seen in Cu-Al-Ni SMAs when 13.3 wt.% Al and 4.3 wt.% Ni was added. A steady shift from $\beta`_1$ to

$\gamma`_1$ via a $\beta`_1 + \gamma`_1$ in the martensite of Cu-Al-Ni alloy occurred when the proportion of Al increased [72, 78]. Volumatic percentage of $\beta`_1$ phase was found in $\gamma`_1$ martensite at a high cooling rate. However, if the cooling rate is too slow, $\gamma`_1$ martensite is formed. It is impossible to avoid forming martensite if the Al concentration is more than 14.2 wt. %. Intermetallic compounds with Al are formed when the matrix of Al diminishes, culminating in the development of $\beta`_1$ martensite in the Cu–Al–Ni alloy base. There will be large martensite plates when the Al content is less than 11.9 wt percent. When the aluminum level reaches 11.9 wt.%, fine plates of $\gamma`_1$ martensite develop. Cu-13.03wt% Al-4.09wt% Ni [79] and martensite primarily produced the M18R type with an orthorhombic structure [80] exhibiting $\beta`_1 + \gamma`_1$ mixture. Figure 2.8 shows that the amounts of Al and Ni in the precipitated phase have a more substantial impact on the morphology of the precipitated phase than previously thought by Chentouf et al. [81] in their study of hypoeutectoidal Cu-Al-Ni shape memory alloys.

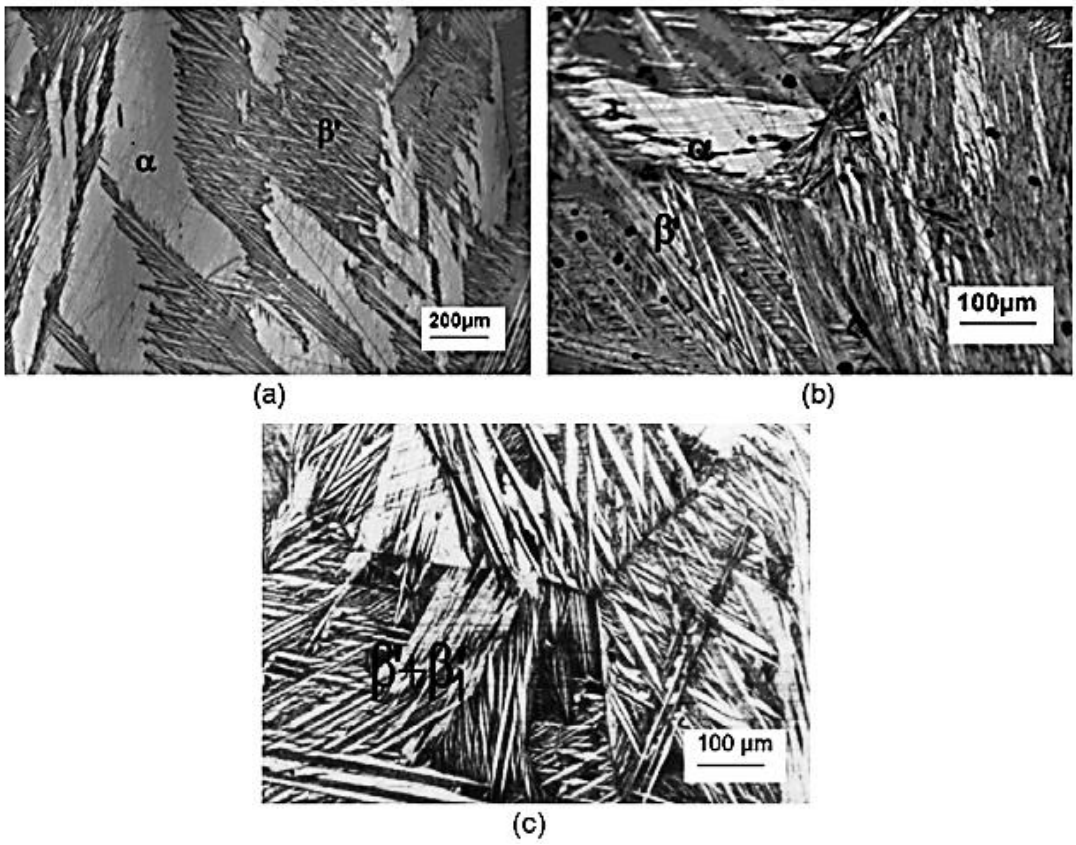

Figure 2.8. Optical micrographs for alloys: (a) Cu-9.9wt. % Al-4.43 wt. % Ni, (b) Cu-11.25 wt. % Al-4.07 wt. % Ni and (c) Cu-11.79 wt. % Al-4.37 wt. % Ni [81].

The 2H martensite at the precipitate matrix/precipitate free contact, large precipitate particles develop in Cu–Al–Ni shape memory alloys. Ratchev et al. [64] indicated that the tensions surrounding the precipitates would alter, resulting in a new 18R sequence. According to Karagoz and Canbay [49], increasing the proportion of Al addition causes the phase to completely martensitic alloy changes the β_1' and γ_1' phases during homogenization, resulting in V-shaped grains with various orientations. Al content of 13 wt.% resulted in self-accommodating groups of zig-zag groups in Chang [50], while martensite with an 18R structure is typical $\beta`_1$ martensite, as illustrated in **Figure 2.9a**. According to **Figure 2.9b**, they are raising the Al content in the matrix to 13.5 wt.%, there are many more coarse variations of $\gamma`_1$ (2H) structure (b). The microstructure grew clearer, showing a β`1 (18R) or $\gamma`_1$ (2H) martensite coupled with the copious precipitate of 2 phase, as seen in Figures 2.6c and (d). The $\beta`_1$ (18R) and $\gamma`_1$ (2H) martensite should coexist in Cu–13.7Al–4Ni SMA, whereas only $\gamma`_1$ (2H) martensite exists in Cu–14.0Al–4Ni SMA, according to Recarte's positive reaction to the range of martensite's and composition. of Cu–*x*Al–4Ni SMAs [72, 73, 82].

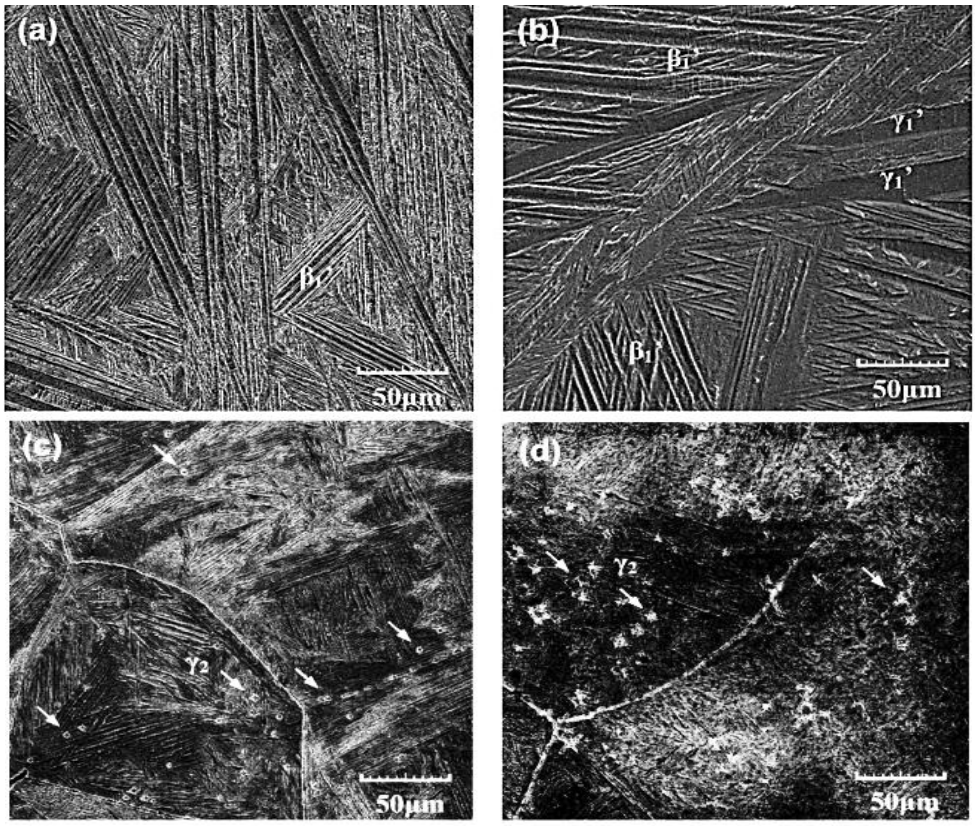

Figure 2.9. Images of SEM [71] of; Cu–13 wt.%Al–4wt.%Ni SMAs (a), Cu–13.5wt.%Al–4wt.%Ni SMAs (b), Cu–13.7wt.%Al–4wt.%Ni SMAs (c), Cu–14 wt.% Al–4 wt.%Ni SMAs (d).

2.3.2. Cu-Al-Mn SMAs

Another category of copper-based SMA is called Cu-Al-Mn [83]. The shape memory effect, transformation temperature, and mechanical qualities have been investigated using this combination, which has been the subject of many investigations. Because of the microstructure management, such as grain size, Cu-Al-Mn demonstrates outstanding ductility, effective damping properties, and magnetic properties. The crystal structure and the lattice parameter of the Cu-Al-Mn compound were effectively altered by adjusting the milling duration and RPM during the ball milling process. The longer the milling process takes, the smaller the grain size ultimately becomes. According to another study, the maximum logarithmic decline occurs when the temperature of the surrounding environment rises. The addition of ternary and quaternary alloys affects the grain size and shape memory effect. Adding up to five percent of aluminum and one to three percent of each zinc, silicon, lead, nickel, magnesium, chromium, and titanium as quaternary elements cause the transformation temperature to rise. The adding of zinc, gold and or silicon to the ternary alloy of Cu73wt.%–Al17wt.%–Mn10wt.% that lead to stabilize the martensite (6M) phase, which resulted in an increase in the Ms temperature. On the other hand, the addition of silver, cobalt, iron, tin, chromium and/or titanium served to lower the stability of the martensite phase, which resulted in a significant reduction in the Ms temperature but an increase in the ductility of the material [84, 85]. It was discovered that when Zn and Ni are added as quaternary additions, grain size expands from austenite to martensite when the temperature is lowered. Still, it contracts when the temperature is raised. The significance of adding Ce lies in that it refines the grain and leads to the production of a Ce-rich phase. This causes the tensile strength and damping capacity to be increased to their maximum levels. The aging study was carried out on Cu-based SMA at temperatures ranging from 800 ^{o}C to 950 ^{o}C, and it found that an increase in temperature led to a rise in damping. The Al content of the material ranged from 11.4 to 12.3 wt.%, and the Mn content was between 5.0 and 6.9 wt.%. It was found that in the same content when silver was added at a concentration of 3 wt.% and then quenched at a temperature of 1127 ^{o}C, it dissolved completely with the mixture. However, a rich quantity of silver precipitates was formed when silver was quenched at a temperature of about 527K. The Ms temperature may be brought down during the

quenching process by adding Nitrogen, which also results in an improved shape memory effect.

The materials that were tested had a higher Ms temperature but a higher hardness after having 1 percent of manganese and Aluminum added. According to the findings of the study on the effect of grain size, the effect of ratio of d/D grain size (where d and D are the grain size and wire diameter, respectively) on the pseudoelasticity and yield stress as increases as d/D increases, and the loading rate and temperature can also be modified by changing the diameter ratios. These findings were discovered after the study on the effect of grain size [86].

2.3.3. Cu-Zn-Al SMAs

Cu-Zn is one of the ductile pairings combined with a certain %wt. It becomes brittle if the base metal is more than 30.5 wt.% Cu. Copper-based alloys are the subject of much study and experimentation in recent years. Many alloy compositions, quenching conditions, heat treatment processes, mechanical deformation, and grain refinement have been tested. Microstructural characteristics and structure hinder the applicability of a cheap synthesis method like Cu-Zn-Al. Two samples were used to optimize the composition of Cu-Zn-Al SMA for vehicle use. The findings show that 70 percent copper, 26 percent Zn, and the remainder Al are sufficient for the application. It is possible to utilize this SMA in other applications, such as actuators. Compared with this technique, other methods can only synthesize the α+β phase. After the β phase, irradiation process loops, cavities, and vacancies can be stabilized, and a closed pack phase can be formed. Still, the formation of single γ crystals decreases when the constant external stress is applied during aging. Austenitization has also been shown to have affected the precipitation of the phase. A Cu-Zn-Al thin layer was formed using a sputtering method and argon gas [87]. An L21 structure with an 18R structure was seen in the martensite β phase, as revealed by films taken throughout the phase—effect of shape memory. For the first time, the shape memory effect was created using the sputtering procedure, and flaws may be stabilized using quenching. The characteristics of shape memory alloys may be altered by temperature based on the martensite-austenite phase change.

There are two possibilities for obtaining the 2H martensite structure, one of which is by setting the electron concentration per atom (e/a) to 1.53 and by obtaining films with an 18R martensite structure in which the hysteresis percent is increased over bulk samples. Nanowires constructed of Cu-Zn-Al from 1-butyl-1-methylpyrrolidinium bis (trifluoromethyl sulfonyl) imide ionic liquid were first described in Ref [88]. The $Cu_{1-x}Zn_{1-y}Al_{1-z}$ shape memory alloys microstructure has been studied and found significant variations in the pseudoelastic and shape memory effect within the range of x is (0.29-0.30) wt.%, y is (0.74-0.75) wt.% and z are (0.83-0.96) wt.%. The shape memory effect is enhanced when the Zn content is increased by 13%, and the Al concentration is increased by 12.9%. Cu-Zn-Al alloys contain Mn and Zr as additional alloying materials with good mechanical performance, high tensile strength, and high ductility. To prevent martensite stabilization, the alloy exhibits strong thermal stability against aging. Thermal conductivity changes when Zn and Al are held constant. When Ni content is less than 2% wt, the transformation temperature is dropped, and it rises again when Ni content is more significant than 2%. wt. For alloys with transformation temperatures below 347K, the shape memory effect (SME) is higher by 20-40% than those with transformation temperatures above 361K [89]. The disordered structural transition from BCC to the FCC phase can be used to explain the martensite transformation. Elongation and tensile strength are increased by 50% and 130%, respectively, when 0.1 wt.% of Boron is added to Cu-14 wt.% Zn-8 wt.% Al. Adding boron also improves the ductility and strength of the material. In all Cu-Zn-Al-X elements studied, the shape recovery rate ranges from 88% to 97% but entirely depends on the quaternary elements [90]. The quaternary element of 0.1-0.4 wt.% Ni was added to demonstrate the alloy's dampening properties and grain refining [91]. Amounts up to 0.4% Ni solidification is directed, decreasing damping capabilities, but at 0.2 wt.%, the damping capacity is at its highest. A reduction in grain size due to the addition of 0.25 wt.%Ce aids in fatigue fracture resistance, which is dependent on microstructural characteristics, loading conditions, and the critical role performed by austenite and martensite transition [92]. The addition of Gd in the 0.08–0.12 wt.% range has a strong shape memory effect that assists in producing helical springs, but there is no change in the martensite transition temperature. Although the shape memory effect is reduced by adding Ti and Zr, and Co can fine-particles the grain size [93]. Temperature-controlled diffusion and expansion of an anaerobic martensite

phase are regulated by the restraints imposed by phases scattered along new α martensite variations' boundaries, and the two-way effects were investigated extensively.

2.3.4. Cu-Al-Be SMAs

The methods previously outlined can also be used to synthesize Cu-Al-Be alloys. Samples with varied compositions examined and step quenched, and aged up to multiple temperatures, found that great attention must be given to avoid oxidation during the first high-temperature stages. Cu22.7 at. % Al-3.1 at. % Be, manufactured via the ingot route, has been studied for its precipitation properties. After homogenization, the ingots were water quenched to get the metastable phase at room temperature [94].

Under isothermal circumstances, XRD reveals the existence of ($\alpha+\gamma_2$) phases. SEM and optical microscopy, on the other hand, report discontinuous precipitation. Increased loading in martensite temperatures diminishes pseudoplastic characteristics, and the crystal orientation determined by EBSD shows homogeneous stress distribution throughout the sample [95]. It was chosen for the corrosion test, which involved keeping the sample in NaCl solution and using X-Ray diffraction to analyze the findings. When immersed for an extended period of time, the single-phase was corroded; however, in the microstructure ($\beta+\gamma_2$), the β matrix is protected from dealloying by γ_2 precipitates. The effect of grain size on Ms temperature in phase Cu-11.41Al0.50Be [96] was examined (weight percentage). As the grain size reduces, the Ms temperature decreases the stress increases. The form memory effect of alloys is affected by aging treatment, as evidenced by tests on diverse samples with varying compositions. The harder an alloy becomes, the longer it has been used. As the aging time increases, SME strain recovery reduces owing to precipitation [97]. Even after aging at 250 ^{o}C and 500 ^{o}C, the SME may be stabilized to a certain extent by adding the quaternary element Mn. It also has a poor damping capability when Mn is added to the alloy. The ultimate tensile strength of the quaternary element alloy is 630 MPa, which is extremely near to the typical Ni-Ti SMA's 800 MPa and excellent hardness

exceeding 200 BHN. Three main factors contribute to wear characteristics: abrasive, adhesive brinelling, and surface fatigue [98].

2.4. DEFORMATION OF SHAPE MEMORY ALLOYS

The martensitic deformation of material causes the shape memory effect (< M_f). Deformation can cause macroscopic shape changes in copper-based alloys. Essentially, the thermoelastic martensitic structure comprises self-adjusted plate variations that merge and reorganize during deformation. This method can also produce identical mechanical twins. Because of this, frequently oriented martensite variations occur due to the applied stress. Austenite martensite transformations can also occur in reaction to deformation, whereas martensite transformations entail variations in the stacking sequence of closely packed planes. Research into martensitic deformation is critical to understanding the shape memory effect's inception. In addition, understanding the tensile and compressive behavior SMAs is critical for recognizing their usefulness in various applications. Both Schroeder and Wayman agreed that the creation of martensite and its subsequent deformation are responsible for martensite's characteristic shape in CuZn alloys. It has been shown that at certain stresses, martensitic interfaces may move in some SMAs, which is an interesting discovery. The martensitic transformation of CuAlNi SMAs, as well as their mechanical and thermoelastic properties, have been investigated under tensile stresses; however, investigations on the material's behavior under compressive pressures are limited.

Several factors determine the mechanical characteristics of SMA, which are influenced considerably by temperature and phase distribution [99]. As a result, the mechanical qualities are inextricably linked to the operational features. In order for a thermoelastic martensitic transformation to be reversible, one of the essential characteristics that must be met is that the stress necessary to detwinned or reoriented (dt) must be less than the yield stress. It is essential to the process that this step be completed correctly so that the material does not suffer from residual stresses and/or plastic deformation, in which both of which are detrimental to the SME. Moreover, thermomechanical metrics like hysteresis, transition temperatures, recovery stress, and capacity of

damping characteristics whereby will be intimately connected to the material's microstructure and composition. For instance, thermomechanical conditions might promote or hinder phase change. Thus, these qualities have a wide range of values based on the combination of the above criteria. These temperatures and hysteresis range from 200 ^{o}C to 400 ^{o}C and 20 ^{o}C to 40 ^{o}C in the Cu–Al–Ni SMA system. Damping capacity is between 10 % and 20 %, considering energy dissipated by the provided energy. The rolling of Cu-Al-Ni SMAs on their microstructure and mechanical characteristics was researched by [100], as illustrated in **Figure 2.10.** For Al10.7 alloy samples, the irrecoverable strain increased fast with the number of heat cycles during SE fatigue cycling. However, this was not the case for samples of Al13.7 wt.% or Al 12.7 wt.% alloy. Additionally, it was shown that the increase in grain size is normally limited by the ultimate thickness of the shape memory alloys ribbons. In addition, the SEM analysis demonstrates that the number of grains in the section as well as their size are a function of the sandwich's initial thicknesses and the number of layers in it. The use of a master alloy in the production of the strips, the cold bonding (Figure 2.11) of the metal layers during the first rolling pass, and the plethora of diffusion phases all contribute to the simplification of the cold rolling process.

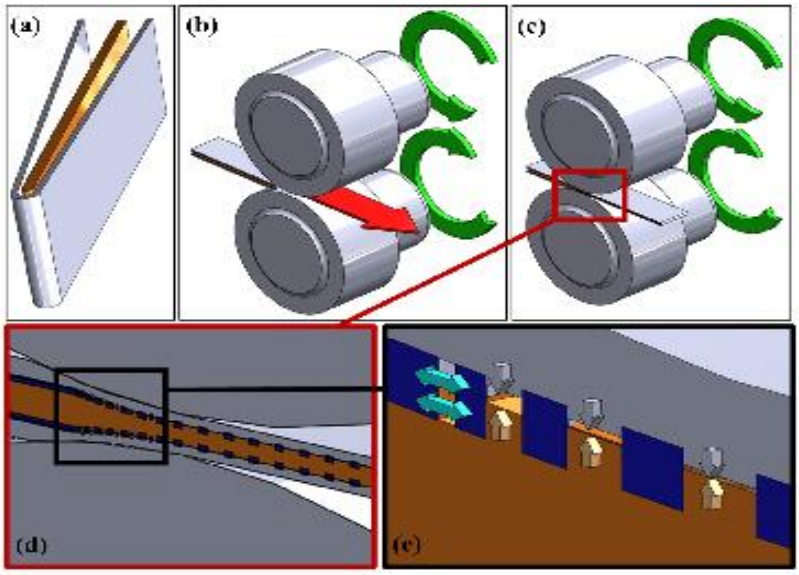

Figure 2.10. An example of the cold rolling process in the form of a schematic: a metal sandwich made up of just two components, b and c; the first cold rolling pass; d and e; a welding mechanism that takes place throughout the process: The brittle layer is shown to be peeling away in the direction of the horizontal arrows, while the healthy material is shown to be extruding in the direction of the vertical arrows [100].

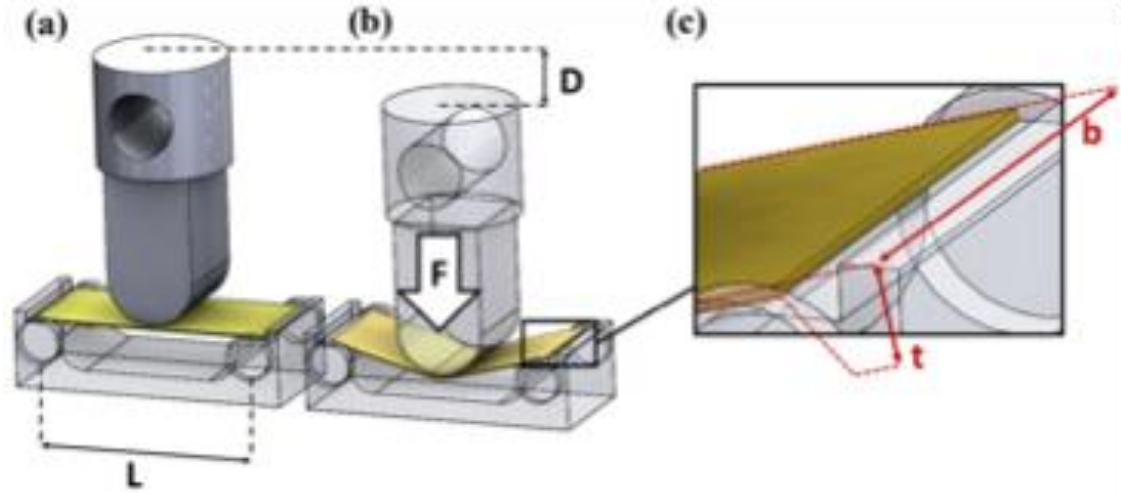

Figure 2.11. Three-point bending set-up: an unloading configuration, b loading configuration, c details of the SMA ribbon [100].

2.5. APPLICATION POTENTIAL

The primary function of a SMA application can be used to classify the application into one of four categories [101, 102]; the SME can be used to produce movement and/or force, and the SE can store the deformation energy [103]. In general, these four categories may be used to classify shape memory applications, such as control, aerospace, automation, automotive, energy, heating and ventilation, chemical processing, safety and security, and electronics applications are just some of the sectors that have developed novel uses for SMAs as a result of their distinctive properties (MEMS devices). Some of these applications use procedures, concepts, or approaches analogous to those used in other domains and may thus be implemented there.

As sensors and actuators, commonly produced binary NiTi SMA covers the vast bulk of automotive applications, including contemporary automobiles. This is since its operating temperature range falls within the usual range of ambient temperature variations to which a passenger car may be subjected while in service (i.e., about -40 ^{o}C to 125 ^{o}C) [104, 105]). The standard binary NiTi SMA has transformation temperatures ranging from -50 degrees Celsius to approximately 110 degrees Celsius [101], and it performs very well for multiple cycles within vehicle locations that fall within this temperature range [105]. However, it does not perform well in locations

with higher temperatures, such as under the vehicle's hood. In order for the SMAs to function correctly, they need to have a M_f temperature that is significantly higher than the maximum working temperatures (note the red dotted lines in Figure 2.9). A comparative of the transition temperatures of the most prevalent SMAs presently under development may be seen in **Figure 2.12**. This comparison reveals that the more affordable Cu-Al-Ni SMAs can perform the transformation at temperatures as high as 200 degrees Celsius; however, these SMAs are fragile, unstable, and have a poor fatigue strength; as a result, using them in many cycle operations is not recommended. [101, 105, 106]. Even though there is a large variety of HTSMAs available, the cost of these materials is still prohibitive for use in automotive applications [105].

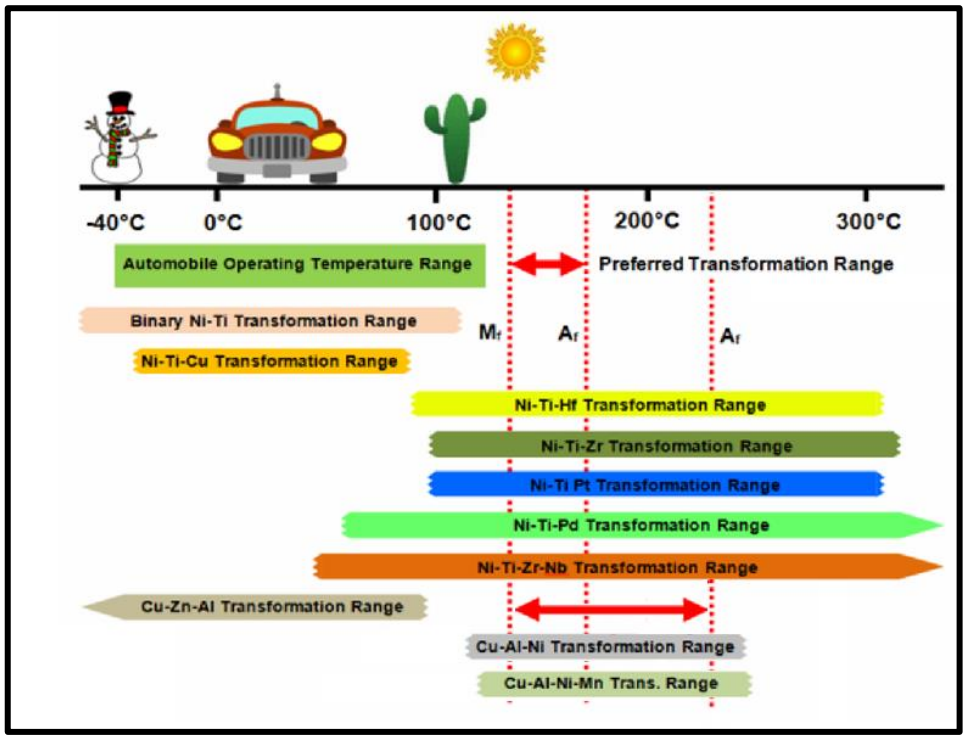

Figure 2.12. Temperature ranges for several commercially available and custom-developed SMAs used in automotive applications [101, 105, 107].

Primarily as artificial muscles and/or micro-actuators, SMAs have been used in several robotic systems since the 1980s [108-110], as reported by Furuya and Shimada [111] and Sreekumar et al. [112]. The majority of shape memory alloys robotic applications in use today are based on biological principles (called as biomechanics). While they are mostly put to use in the biomedical industry, they are also put to substantial use in various other industries. The problems consist of boosting the performance of the

hardware platform while simultaneously decreasing its size and raising the level of intelligence possessed by the integrated system (i.e., smaller, faster, reliable, and autonomous). Several technical problems have been identified and need to be fixed. These include difficulty with clamping for micro-robots as minuscule electrical connection, low electrical resistance, low output of strain value, challenge in controlling and minimum value of efficiency. The selection of appropriate modeling tools, control mechanisms, and feedback sensors, on the other hand, has allowed for the resolution of some of these problems. As an illustration, the resistance feedback control is excellent for tiny robots since it does away with the requirement for extra sensors, even though its precision is restricted [112].

As been said previously, the reaction rate of the SMA actuator is highly dependent on its form and size. These characteristics have a considerable bearing on the total dimensions of the robotic device and the number of degrees of freedom it possesses. In most cases, resistive heating is employed for SMA actuators on the smaller side (up to 400 m in diameter). In contrast, indirect heating approaches are utilized for actuators that are on the larger side [112]. Capacitors are included with thicker actuators to produce a quick heating response, which allows for an increase in actuation frequency. Several cooling techniques may be implemented, as was noted before, to optimize the cooling process, but they would make the device larger [112]. In addition, the number of robot actuators needs to be raised to enhance the degrees of freedom they possess, which results in complicated control issues.

Bridges that vibrate might experience severe strains as a result. One example is the vibration caused by wind acting on the wires that hold up suspension bridges. It has been demonstrated that shape memory energy absorbers (such as NiTi and Cu-based SMAs, for example) can successfully dampen vibration [113, 114]. An investigation of earthquake damage and the ways in which buildings may be strengthened to withstand high levels of seismic vibration was funded and carried out with the assistance of the European Union. A model of a structure with four stories was made out of shape memory tendons, and the tendons were positioned in such a way as to reduce the amount of structural damage that an earthquake would cause. The model was subjected to shocks mimicking the vibration profile of a recent earthquake after it

was placed on the shake table in Greece, which holds the record for being the world's most enormous shake table. A building model that had not been changed with SMA devices was demolished, but a model that had been modified with these devices survived with minor damage.

As a consequence of these studies, the basilica on the shrine in Assisi, Italy, which had been nearly devastated by a previous earthquake, is being reconstructed with SMA tendons to decrease the damage that subsequent earthquakes will cause. The tendons are able to absorb energy by utilizing the superelastic effect, and they are also able to offer a moment of righting after the shock wave has gone through the body. A number of other SMA devices have been developed to rehabilitate structures damaged in the California North Slope earthquake that occurred a number of years ago. Compared to the alternative method of re-welding the connection, using a shape memory couple to repair the failed welded beam to column joints can result in significant cost savings. An SMA repair method has also been developed for the concrete columns that support the above highway. Before wrapping it towards the column and securing it, a cable made of shape memory alloys would first need to be pre-stretched to the proper length. After being heated by the passage of electric current, the cable might contract, imposing a large compressive stress on the column, and therefore returning the column to the original condition of structural integrity it had [114].

The use of shape memory tendons in pre-stressing or post-stressing concrete constructions [113] is a technique that, like earthquake damage mitigation, reduces the severity of the damage. The conventional procedure involves sustaining the strain by means of large abutments while stretched high-strength steel tendons over the ends of a beam built of concrete. Only after cement has been applied and given time to harden, the tension that was placed on the steel tendons is released. This causes the concrete to become more compressed, which considerably enhances its ability to support loads. Because of the need of using enormous jacks and weighty steel abutments on the building site, things are certain to become quite difficult. One alternative method that is now being contemplated involves the pre-stretching of shape memory alloy tendons at a shop before transporting them to the building site in the same manner as conventional reinforcing rods are brought there. It before concrete is poured at the

building site, the rods are positioned in the appropriate pattern in the concrete molds using the construction blueprints.

The thermos-responsive Cu-based SMMs have been at the forefront of current progress, with the addition of fresh materials and techniques taking place on an ongoing basis. There are many ways in which the performance of manufactured things like materials and buildings might be improved or given a new dimension. In recent years, there has been an expansion in the variety of applications for SMAs; the medical industry, the aerospace industry, and the marine industry are the primary users of SM components. Actuators and sensors are the most common applications for copper-based SMMs; nevertheless, these components may also be used in various engineering devices because of their unique features. SMMs can also be used as superelastic devices, such as antennae for cellular telephones, eyeglass frames, and medical devices, including catheter guide wires, dental arches, and stents. These applications are in addition to their usage in engineering equipment. The development of actuators has not kept up with the rise of super-elastic applications. The use of shape-memory wires has been particularly welcomed in medical applications; nevertheless, developing tiny implantable devices is not yet at an advanced stage. Every application is driven by the cost of production, except for those involving space utilization. Micro-actuation is a substantial divergence from traditional actuators. Emerging industries in the field of micromachining are anticipated to benefit from the growth potential presented by microvalves and micro relays. Miniaturization will continue. The primary motivating factors are required to attain minimal internal capacity, mobility, and cost-effectiveness. The integration of components will eventually result in analytical tools and consumer goods that are the size of a pocket [115]. When better materials become available, it is anticipated that the range of applications for SMMs will likewise expand. These include:

Engineered constructions could function to their structural and performance confines without worrying about exceeding either. Maintenance engineers would be able to see the whole performance history of these buildings, as well as the exact position of any problems, while also being able to oppose undesirable or possibly dangerous circumstances such as excessive vibration and performing self-repair [116].

a) Aerospace: 'Sensual devices' refers to materials and structures used in aerospace applications. It is possible to build structures that can sense their surroundings and create data that can be used for health and usage monitoring. Composite constructions will be able to communicate their life histories, including their strengths and weaknesses, to intelligent materials systems, allowing for a "graceful retirement." [117].
b) Civil Engineering Applications: Even in high-tech fields, such as aircraft, the use of "sensual structures" is not limited. They could be used to examine the long-term longevity of civil engineering structures [116].
   i. Monitoring a bridge's present and long-term behavior would increase its safety by revealing structural flaws early enough to be repaired. When employed with structural restoration, it can monitor the structure beyond its intended life safely. This would extend the bridge's safe usage.
   ii. ‘A wide range of home uses for 'sensual' materials and structures include packaging material tracking safe storage and cooking.
   iii. Piping: Using the material's constraint attribute to ensure a better fit and no leaks.
c) Adaptive materials: SMMs or alloys (SMAs) are one type of smart material that may be used to create structures that can perceive and adapt to their surroundings. Adaptive materials and structures have the capacity to move, vibrate, and display a variety of different real-time reactions in addition to the sensory characteristics mentioned before.
d) The automobile sector eagerly awaits intelligent materials technology. As a result of these projects, smart vehicle seats are being developed to recognize the primary occupants and adjust to their height and leg room requirements. Cars can also notify owners how often air pressure their tires to have when they need an oil change, as well as other maintenance information thanks to new technology—cutting expenses by developing solid-state and smart-material technologies [118].
e) Mechatronics: Hybrid mechanical and electrical systems are known as "smart materials" in Mechatronics. These materials use atomic or molecule sensing and actuation to perform their functions.

f) Robotics: Due to their negligible weight, these materials are commonly used in robotics [119].
g) Medicine: However, because of its superior biocompatibility in fields such as dentistry, blood-clot filter, intervertebral disc connector, and actuated implanted drug delivery system, Ni-Ti alloys are reserved primarily for medical applications. Although biocompatibility is not a concern in some circumstances [120], Cu-based SMAs can be used. These include:
   i. Optometry: It is common for these frames to be constructed using SMAs with a lower transition temperature than the ambient temperature. As a result, even when subjected to high stress, the frames retain their original shape once the metal has been unloaded. When under load, the crystal structure can undergo a transformation known as the stress-induced martensitic effect. This allows the shape to shift briefly. This means that SMA-based eyewear is more resistant to being destroyed by accident.
   ii. Medical accessories: An example of Wagner's thermolock, where sterilization containers are locked with an SM spring. SM spring seals the container during sterilization, and once opened, the thermolock must be resealed using sterilization.
h) Defence: Bulletproof vests made from shape-memory alloys will be more comfortable and lighter.
i) Fluid Connectors: SMAs are used to join pipes in SM coupling. It is typical to employ an alloy sleeve that is usually smaller than the pipe it joins. Because of the memory effect, the sleeve returns to its former size, resulting in an extremely snug fit.
j) Coupling: SMA technology is used to manufacture a variety of cryogenic tubes as well as pipe couplings for the aerospace sector. These couplings are used to provide persistent metal-metal seals on aeroplanes.
k) Valves and various kinds of safety measures are available.
l) SMAs have been around for a long time. Still, they have not been widely employed in the construction business until lately because of their high cost, poor elasticity modulus, and lack of expertise in the civil engineering profession, for instance:

i. Retrofitting
ii. Repair of a section of a pedestrian overpass that had developed cracks for the highway bridges applications RC beams reinforced with SMA rebars
iii. SMA is an abbreviation for short fibre reinforced cement material.

m) It is also worth mentioning that certain alloys, such Cu–Al–Mn-based SMAs, are more suited for specific applications than others. Because SMAs based on Cu–Al–Mn have strong SM properties and outstanding ductility, their application in various applications is greatly anticipated [121].

CHAPTER THREE

EXPERIMENTAL

This chapter provides a comprehensive account of the experiments that were carried out in order to achieve the goals that were set. In addition, the process of casting incorporates phase detection methods such as differential scanning calorimetry (DSC), optical microscopy (OM), scanning electron microscopy (SEM), and x-ray diffraction (XRD). There is additional information supplied about the mechanical testing that was conducted, which included hardness, tensile, and shape memory effect tests.

According to Figure 3.1, the experimental work is separated into two primary phases. The first phase of the Cu-Al-Ni shape memory alloy's base alloy investigation explains the phase change behaviour. The impacts of pre-rolling on Cu-Al-Ni SMA transition temperatures, morphology, and mechanical characteristics will be examined in the second phase.

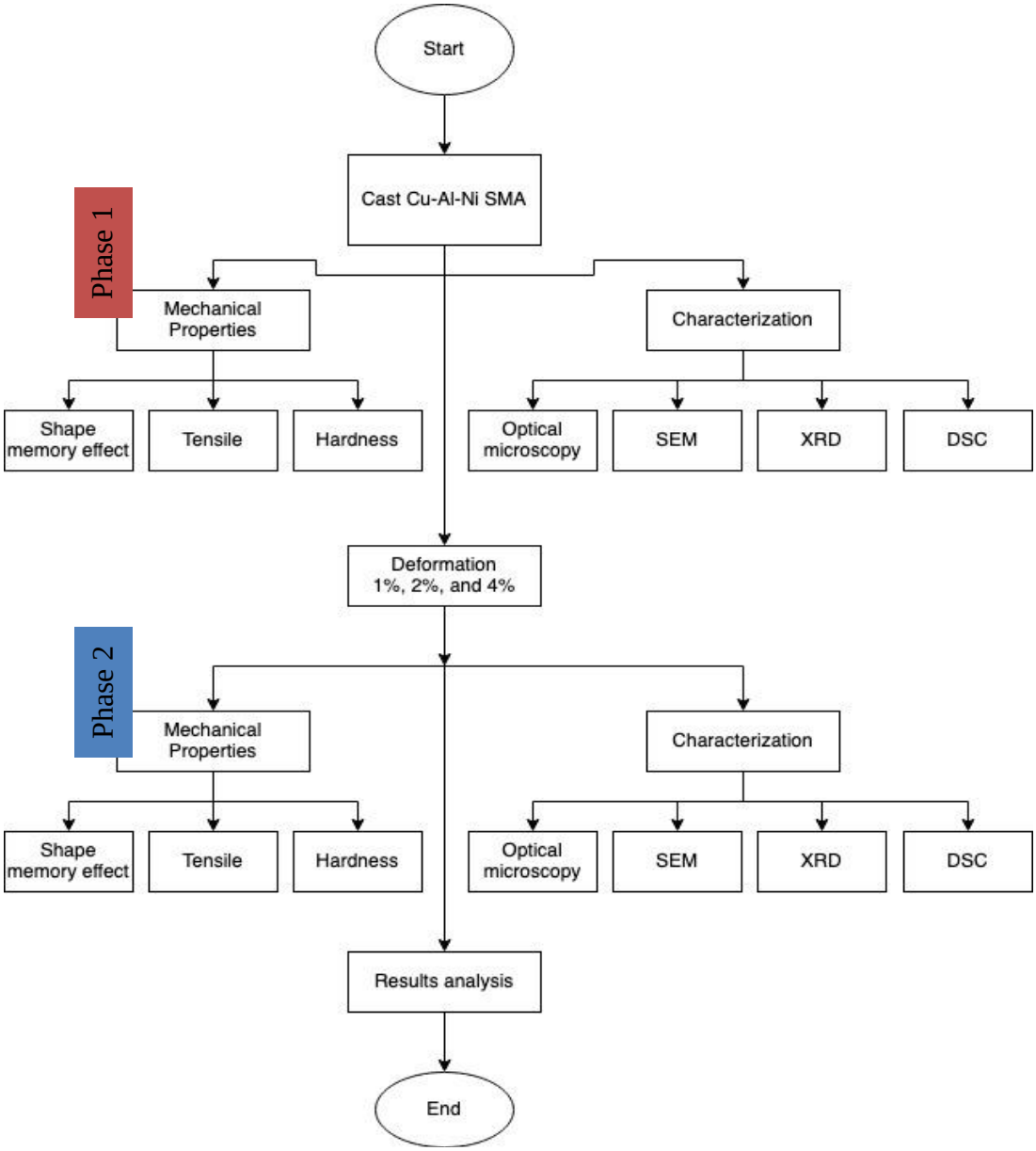

Figure 3.1. Flow chart of the project

3.1. MATERIALS

The material for this project was used as Cu-Al-Ni SMAs with the nominal composition of $Cu_{100-x-y}$-Al_x-Ni_y (where x is 13 wt.% and y is 4 wt.%).

3.2. PRODUCTION OF THE MATERIALS BY CASTING PROCESS

The $Cu_{100-x-y}$-Al_x-Ni_y shape memory alloys were produced by melting high purity metals (Figure 3.2) of Cu, Al, and Ni, respectively, in an induction furnace and then combining the resulting melts. The list of materials and putrity used in this research as well as their respective suppliers are given in the Table 3.1. As depicted in Figure 3.3, these metals were melted in a silicon carbide crucible at approximately 1300 C with constant stirring and then poured into a 270mm x 50mm x 20mm cast-iron mould. The casted sample were wire cut into the dimension of the tensile test specimen according to the ASTM E08 and to the dimension of 10 mm x10 mm x 10 mm for the morphological characterization.

Figure 3.2. The raw materials of Cu, Al, and Ni, supplied by Sigma-Aldrich.

Table 3.1. List of materials and properties.

Metal/Element	Purity (%)	Supplier	Shape
Copper (Cu)	99.999	Goodfellow, UK	Granule
Aluminum (Al)	99.9999	Goodfellow, UK	Granule
Nickel (Ni)	99.95	Goodfellow, UK	Granule

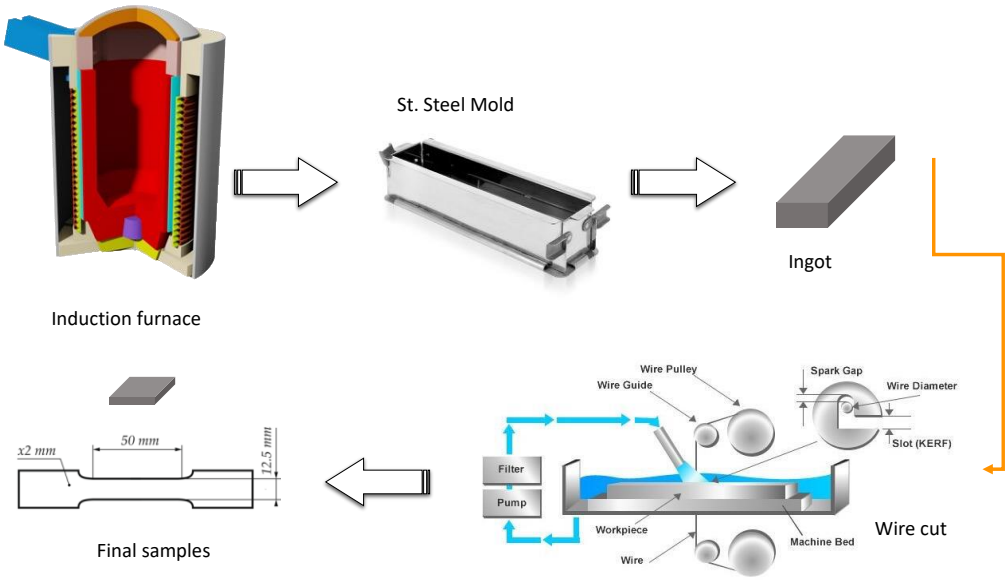

Figure 3.3. Production of the cast and cutting materials.

3.3. HOMOGENIZATION PROCESS

An essential step in the homogenization process is heating and cooling the metal in such a way that a uniform microstructure is formed. For reasons including improving memory effects for form, homogenization of the structure is frequently undertaken after casting. A consistent microstructure is the fundamental goal of the homogenization process. This technique is performed on cast alloys. The homogenization method includes preheating alloys to 850 ^{o}C and a water-quenching procedure to homogenize the casted microstructures. The homogenization furnace is shown in Figure 3.4.

Figure 3.4. Homogenization furnace, ProTHERM furnace.

3.4. DEFORMATION BY PRE-ROLLING

According to this project plan, the deformation process was carried out on the materials sample using the rolling process with different loading and thickness. A load was rolled in the materials sample with the deformation percentages of 1%, 2%, and 4%,. The deformation concept was applied using the rolling process shown in Figure 3.5. This process aims to see the effect of deformation on mechanical and shape memory behaviour. The rolling force on the sample materials places the initial strain on the materials before it goes through any process to see the materials' mechanical and shape memory behaviour before and after the deformation.

Figure 3.5. Rolling machine.

3.5. SAMPLE PREPARATION FOR MATERIALS ANALYSIS AND TESTING

3.5.1. Cutting

A wire cutting was used to cut the casted ingot into the experimental samples with the dimension of 10mm (L) x 10mm (W) x 2mm (t) for the microstructure test, and dimension of 20mm (L) x 10mm (W) x 5mm (t) for the mechanical test.

3.5.2. Grinding

Grinding and lapping are two processes that provide a surface finish that is completely smooth, absolutely flat, and matte. These processes erase any surface deformations, irregularities, and cutting marks.. A finely grounded surface is necessary to carefully analyse light-microscopically low power reflected materials at different magnifications. Subsequent slimming of the SiC abrasives with diameters of 220, 500, 800, and 1000 μm was performed. When the ground surface is transformed from the coarse to the next finer granular size, the loosened abrasives and fine particles from samples created during gross grinding were adequately cleaned.

3.5.3. Polishing

Polishing is a smooth, flat, and scratchless appearance of brilliant, bright, and reflective surfaces. Polishing minimizes the fine imperfections of the surface that remain from the melting process. Polishing occurred based on lubricants in three steps using a polishing machine (Metco). The initial step was to level out the surface using a 9μm long MD-Sat as a 4-minute lubricant. Second, use the lubricant of MD-Dac 3 μm with Dac for four minutes. The three-step is to use the 1 μm MD-Nap with Nap R as a 1-minute lubricant.

3.5.4. Etching

Etching was employed in the selective chemical attack to reveal the metal's microstructure. It also removes the very thin layer that is extremely distorted when molten and polished. A reagent is used to grate the specimen. For example, an aqueous solution that has been saturated with hydrochloric acid and only contains a few drops of it can be used to etch stainless steel or copper and its alloy. A cotton spray wiped on the surface a couple of times is used. The sample should be kept alcoholic and dried quickly. For the project, a 2.5-g (FeCl-3.6H2O) solution and 48-ml methanol in 10 ml HCl is used in the sample for 20 seconds.

3.6. MATERIALS CHARACTERIZATION

This project required several characterization tests such as Optical Microscope (OM), Scanning Electron Microscope (SEM), X-Ray Diffraction (XRD), and Differential Scanning Calorimetry (DSC).

3.6.1. Optical Microscopy (OM)

The optical microscope was used to observe the casted and deformed microstructure of the Cu-Al-Ni SMAs.

3.6.2. Scanning Electron Microscope (SEM)

A scanning microscope (SEM) and energy spectroscopy (EDS) were utilized to investigate the surface morphology of Cu-Al-Ni alloys. The characterization for transmission electron microscopy was conducted to analyze some of the selected alloys' crystallography and morphology. The SEM was used CARL ZEISS ULTRA PLUS GEMINI FESEM (Figure 3.6) attached with EDX.

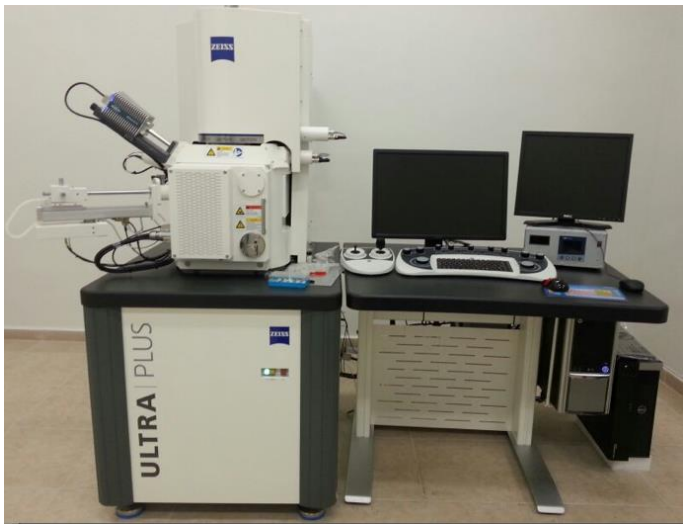

Figure 3.6. Carl zeiss ultra plus gemini fesem.

3.6.3. X-Ray Diffractometry (XRD)

The microstructure analysis using the XRD technique of Rigaku Ultima IV -X-Ray Kırınım Spektrometresi equipment with a CuKα X-ray source (as shown in Figure 3.7) was carried out. A locked couple and scanning step of 0.05 ^{o}/sec were used as a scanning mode in a 2θ range between 10-90^{o}.

Figure 3.7. Rigaku Ultima IV -X-Ray Kırınım Spektrometresi equipment.

3.6.4. Differential Scanning Calorimetry (DSC)

The differential scanning calorimeter using Hitachi Differential Scanning Calorimeter Dsc7000 Series (DSC), as shown in Figure 3.8, was used to determine the transformation temperatures of the Cu-Al-Ni SMAs. These temperatures included the martensite start (Ms), martensite finish (Mf), austenite start (As), and austenite finish (Af). The Hitachi Differential Scanning Calorimeter Dsc7000 Series temperature range is a (-150 ^{o}C - 750 ^{o}C). For the analysis, approximately 2–6 mg of filings comprised the alloys that were extracted using a grinding saw machine.

Figure 3.8. Hitachi differential scanning calorimeter DSC7000 Series.

Figure 3.9 illustrates the typical transition temperatures of the schematic DSC curve produced by the DSC device during heating and cooling runs. The temperatures of transformation were computed with the help of the universal analysis 2000 software programme, and the data obtained from that calculation were plotted with the Magic Plot software. The depicted curves were then fitted with the Gaussian equation to obtain the accurate heating and cooling curves. The Martensite to austenite transformation curves' onset and offset temperatures have been extrapolated and used to establish the transformation temperatures. It was necessary to optimize the heating and cooling rates since excessive heating and cooling rates frequently reduce resolution between adjacent peaks. When the pace of heating or cooling is extremely slow, sensitivity declines, and in some cases, the peak even vanishes entirely.

The temperatures of transformation were calculated with the assistance of a software program called universal analysis 2000, and the data that was produced from that calculation was displayed with the assistance of a software program called Magic Plot. In order to produce the correct heating and cooling curves, the displayed curves were first given a Gaussian equation fit, and then the results were analyzed.

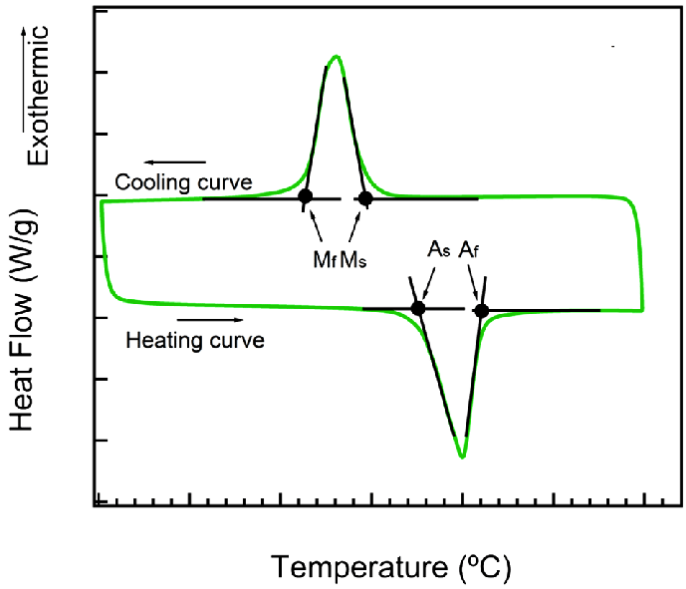

Figure 3.9. Schematic of a typical differential scanning calorimeter curve showing critical transformation temperatures, γ: Austenite; M: Martensite.

3.7. MECHANICAL TEST

3.7.1. Hardness Test

The Vickers hardness test "QNESS HARDNESS MEASUREMENT DEVICE" was used to determine the hardness of the sample materials. The hardness test was carried out using a 10 kg applied load for 30 seconds then the measurement was taken.

Figure 3.10. QNESS Hardness measurement device.

3.7.2. Tensile Test

The tensile strength was measured using the "ZWICK/ROELL Z600 tensile-compression and bending test machine (Figure 3.11) to obtain the stress-strain curves and indicate the failure points. The rectangular tensile specimens were cut into 25-gauge lengths in accordance with the tensile standard E08, and the tests were carried out at room temperature of 26 ^{o}C.

Figure 3.11. ZWICK/ROELL Z600 tensile-compression and bending test machine.

3.7.3. Thermomechanical Test / Shape Memory Effect Test (SME)

A specially designed tensile machine conducted the shape memory effect test using ZWICK/ROELL Z600 tensile-compression and bending test machine shown in Figure 3.11. The strain of the sample was measured after the tensile strain at 2% was obtained, and the final strain of the deformed sample, which was still unrecovered, was then heated above A_f, 600 ^{o}C for 10 minutes and then quenched using a water medium to obtain the detwinned martensite structure. The shape memory effect [122] was measured according to the following equation:

$$Shape\ memory\ effect\ (SME)\% = \frac{\epsilon_i - \epsilon_f}{\epsilon_i} x\ 100$$

Where ϵ_i is the initial strain and ϵ_f is the final strain after heating the sample to a temperature above A_f.

CHAPTER 4

RESULTS AND DISCUSSION

4.1. INTRODUCTION

This chapter shows the results of deforming a sample by 1%, 2%, or 4%. These results show how the sample's phase transformation characteristics changed. The impact of deformation was evaluated using the variations in phase transformation characteristic parameters and microstructural analysis compared to the undeformed sample. The alterations in microstructure were studied using an optical microscope, SEM, EDX, and XRD. On the other hand, tests for microhardness, tensile strength, and shape memory effects were conducted in order to evaluate the material's mechanical characteristics while the deformation was applied. In conclusion, this chapter aims to give a map that illustrates the relationship between the results of phase transformation characteristics and the mechanical qualities that exist along the deformation %.

4.2. MICROSTRUCTURE OF CU-AL-NI SHAPE MEMORY ALLOYS

The Cu-Al-Ni homogenized base alloy microstructure is seen in Figure 4.1. The martensite formed into two different shapes: plates and needles. According to several research, martensite often forms in two distinct types of stacking structures: (i) self-accommodating stacking martensite and (ii) stress-induced stacking martensite with a monopartial structure [123, 124]. Self-accommodating plate-like martensite has a shape called diamond shape morphology, which can make a long-layered structure [125]. The self-accommodating martensite may form six groups, each comprising four varieties. Macroscope morphological changes may be achieved with minimal variation when these variant groups are joined [125-127]. In noble metal copper-based, ternary alloys like Cu-Zn-Al, Cu-Al-Mn, or Cu-Al-Ni, the martensitic microstructures are distinguished by the prevalence of groups of essentially parallel-sided plates and the occurrence of relatively few large groups of unique orientation within the grains of the parent phase [127]. This is the feature that is considered to be the most distinctive aspect of the martensitic microstructure. For Cu-based SMA, the austenitic phase

undergoes two forms of atomic ordering during cooling before the martensitic transformation: the first arrangement, B2, is among the nearest neighbors and is regarded as inescapable even at extremely high cooling rates. The ordering phenomena occur below the ordering temperatures. Despite this, it occurs because there is sufficient driving force for the diffusion of the atoms, which is important to keep in mind, given that this phenomenon is triggered by heat. Because a shift in the local composition and structure of the material significantly influences the temperature range in which a phase transformation can occur, the arrangement of the alloys is becoming a matter of particular importance during martensitic transformations. This is because of the importance that the sequence of the alloys becomes a concern of great significance in the transformation temperature range of this alloy.

The alloys may achieve the shape memory effect due to the martensite variations' ability to undergo plastic deformation even when subjected to relatively moderate stress levels. A very thin layer or two or four plate-like martensite's may be present in the plate-like martensite's. These groups are contacted in order to develop a self-accommodating system based on the crossing plate-like structures, also known as conventional habit planes. On the other hand, the planes of the internal connections are sometimes referred to as a double martensite plane [126-128]. There are two forms of martensite microstructures shown in Figure 4.1b, $\beta`_1$ with an 18R structure and $\gamma`_1$ with a 2H structure. Parallel martensite morphologies in the $\gamma`_1$ suggest that it is a lath structure [129]. The grain also has these sorts of lath morphologies. While in martensitic conditions, the $\beta`_1$ phase is often generated with self-accommodating groups in a needle-like structure [68]. In the as-quenched state, the self-accommodated martensite plate groups are formed. According to Aydogdu et al. [127], continued annealing causes grains to grow.

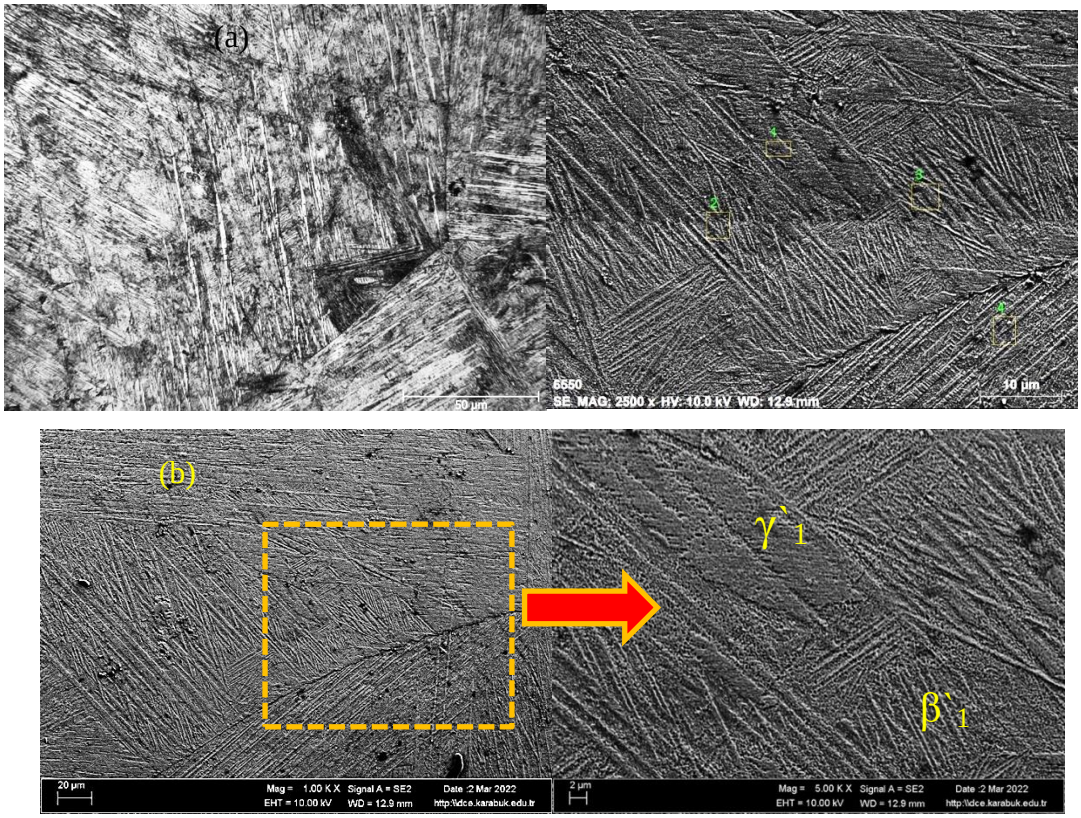

Figure 4.1. Cu-Al-Ni shape memory alloys microstructure (a) micrograph of optical microscopy and (b) Scanning electron microscopy.

As illustrated in Figure 4.2 (a-c) and Table 4.1, the concentrations of the components in the alloy composition of Cu-Al-Ni SMAs are displayed. According to the EDS analysis shown in Figure 4.2 (a–c), the $\gamma`_1$ phase in spectrum 1 had a higher amount of aluminum (12.54 wt.%) and not much nickel (6.16 wt.%). On the other hand, the $\beta`_1$ (M18R) in spectrums 2, 3, and 4 had a lot of nickel (6.58–7.07 wt.%) and not much aluminum (12.23–12.32 wt.%), which shows a distinguished approach for these two phases.

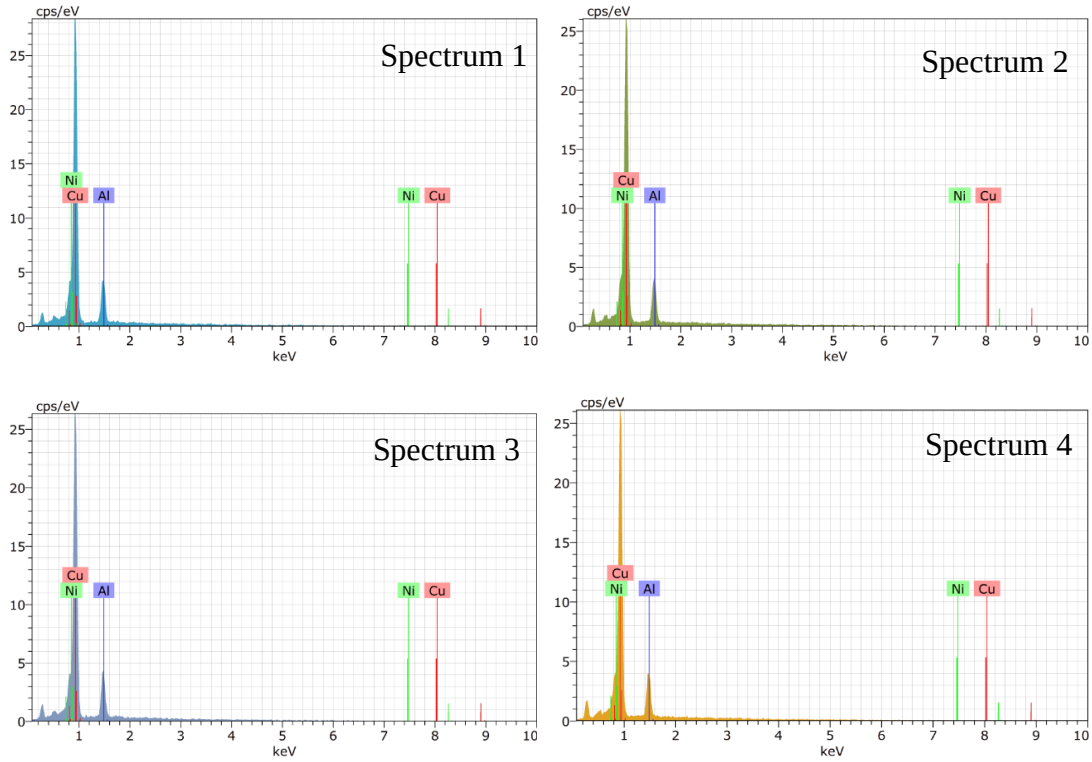

Figure 4.2. EDX spectrums of the Cu-Al-Ni SMAs.

Table 4.1. EDX results of the elemental analysis of Cu-Al-Ni SMAs.

Spectrum	Al	Ni	Cu
	Mass percent (%)		
1	12.54	6.16	81.30
2	12.23	6.77	80.99
3	12.32	7.07	80.61
4	12.29	6.58	81.12

Cu-Al-Ni SMA may be generated in various phases and structures depending on the alloy composition and heat treatment, which have been proven by numerous research [56, 68, 71, 76, 128, 130-138]. Cu-Al-Ni SMA XRD patterns are depicted in Figure 4.3. The M18R martensite was determined to be the most common kind of martensite. Several distinct XRD patterns corresponding to the different phases were identified, for instance: the phase of γ'_1 represented by (200), (202), and (1210), while (122), (128), (208), (320), (040) and (311) belong to phase β'_1 [67].

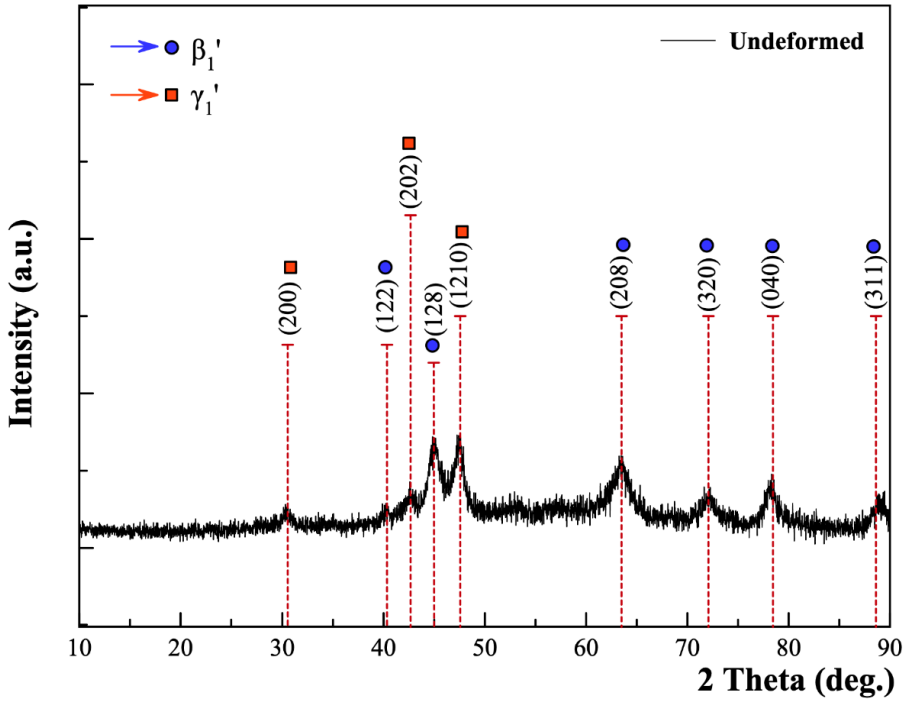

Figure 4.3. X-ray diffraction patterns of the Cu-Al-Ni SMAs.

4.3. PHASE TRANSFORMATION TEMPERATURE

The DSC was used to determine the alloys' transformation temperatures. The extrapolated onset and offset temperatures, shown in Figure 4.4, were used to compute the austenite start (A_s), austenite finish (A_f), martensite start (M_s), and martensite finish (M_f) temperatures and the results are provided in Table 4.2. Even though it is common for thermal analysis to use extrapolated onset and end temperatures, most research has been done on reactions rather than phase changes. DSC curves of diffusionless martensitic transformations may have been better understood if the onset and offset temperatures (the point of divergence from baseline) were used instead of extrapolated temperatures.

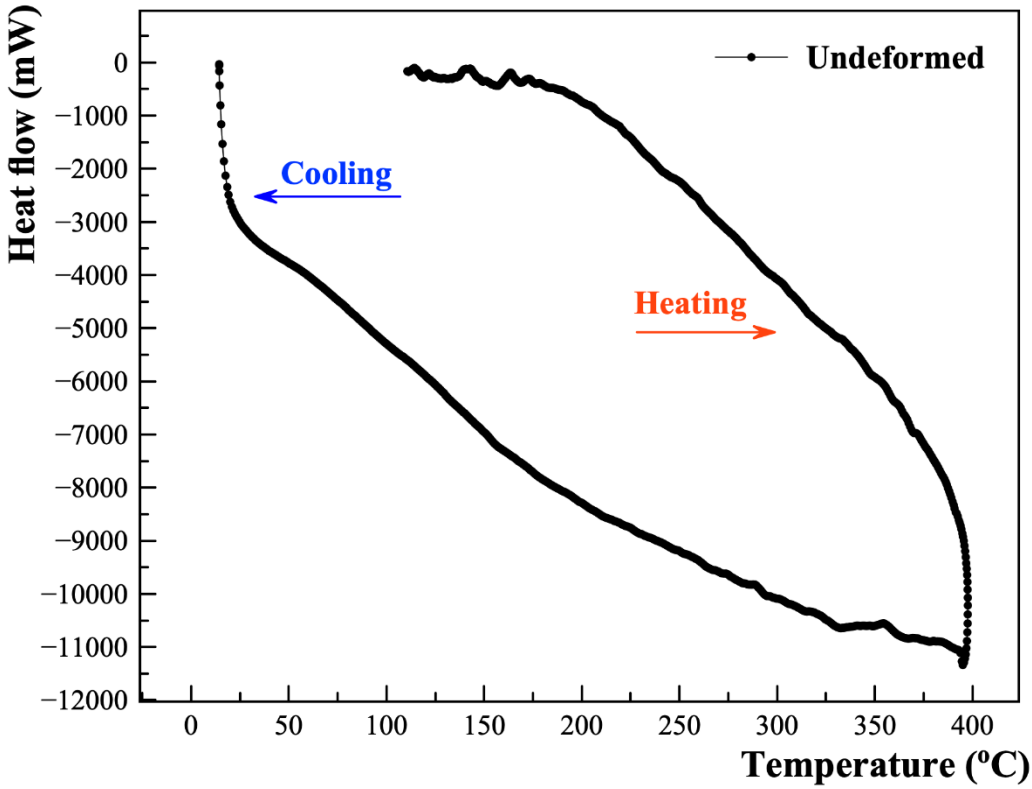

Figure 4.4. DSC curves of the Cu-Al-Ni SMA.

Table 4.2. The Cu-Al-Ni shape memory alloy transformation temperatures.

Transfer Temperatures	A_s	A_f	M_s	M_f
Temperature (^oC)	150.2	168.5	275.8	260.3

4.4. Cu-Al-Ni SMAs MECHANICAL PROPERTIES

4.4.1. Hardness

An average of three different values was used to calculate the microhardness of Cu-Al-Ni SMA, resulting in a value of 346 HV. However, this number is somewhat greater than that of Sampth [68], which can be explained by the difference in the quantity of aluminum, which comes in at 11.39 wt.%, as well as the particular phase structure and grain size that can be seen in the microstructure.

4.4.2. Tensile Test

Figure 4.5 shows the tensile stress-strain curve of the Cu-Al-Ni SMA obtained from the tensile test. It was done at room temperature, and the crosshead moved at 0.1 mm per minute. The measured fracture stress is 5.6 MPa, and the measured fracture strain is 2.1%. Two distinct deformation zones are seen when the alloy is subjected to loading until failure. A non-linear connection between loading and stress and the strain was seen in the first section. The reorientations of the martensite variations in this stage were reported in the non-linear area as these variants were not orientated. As a result, even after increasing the stress, some non-reoriented variations survive [19, 139, 140]. Aside from that, the linear stage is associated with the deformation of the martensite-martensite-driven transformation and the completion of reorientations of remint variations from the first stage.

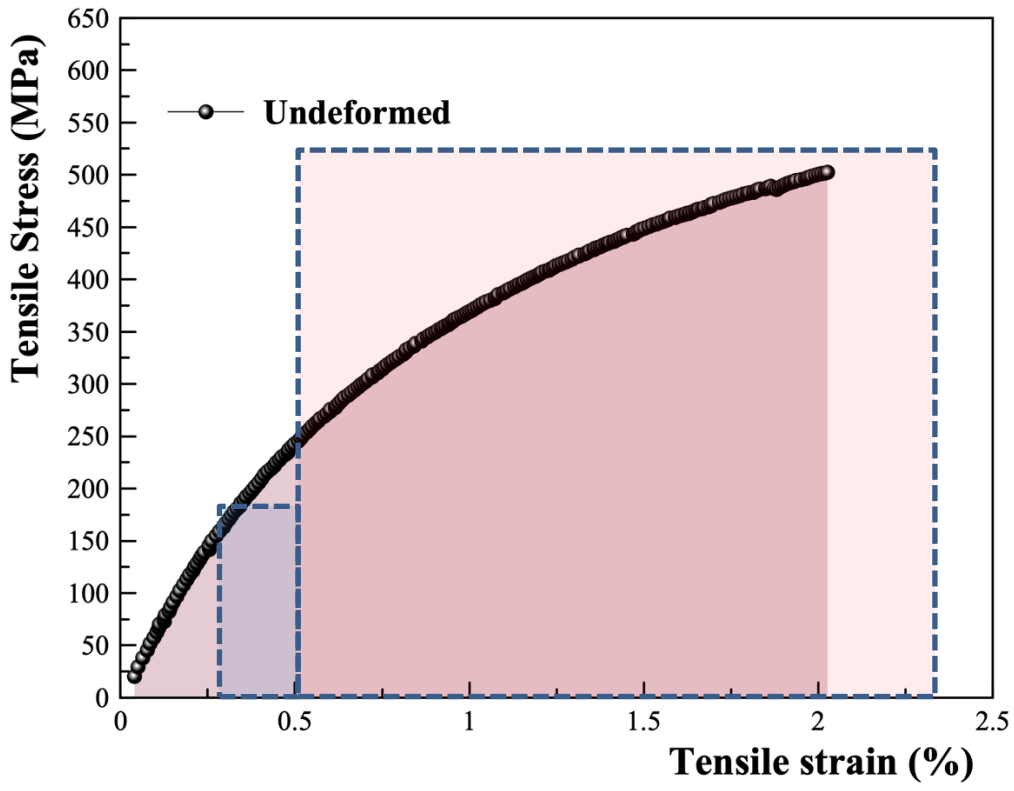

Figure 4.5. The stress-strain curve of Cu-Al-Ni SMAs.

Figures 4.6 a and b depict the Cu-Al-Ni SMA's fracture surface. The Cu-Al-Ni SMA has a brittle fracture mode and can stretch only to a maximum of 2.1 % before

breaking. As observed in the typical casting method, the brittleness of Cu-Al-Ni SMA has been validated by other investigations [16, 141-143]. Remember that cracks always begin at grain boundaries and progress through the specimen at varying angles depending on the direction in which the uniaxial tensile force is applied (see Figures 4.8a and b) [16]. Crack propagation is caused by the complex distribution of stress at grain boundaries, making it difficult for the stress to be released even during the deformation process and elastic anisotropy. However, the crystal orientations associated with the tensile axis cause some martensite. Martensite forms on the other side of grains during the same deformation stage.

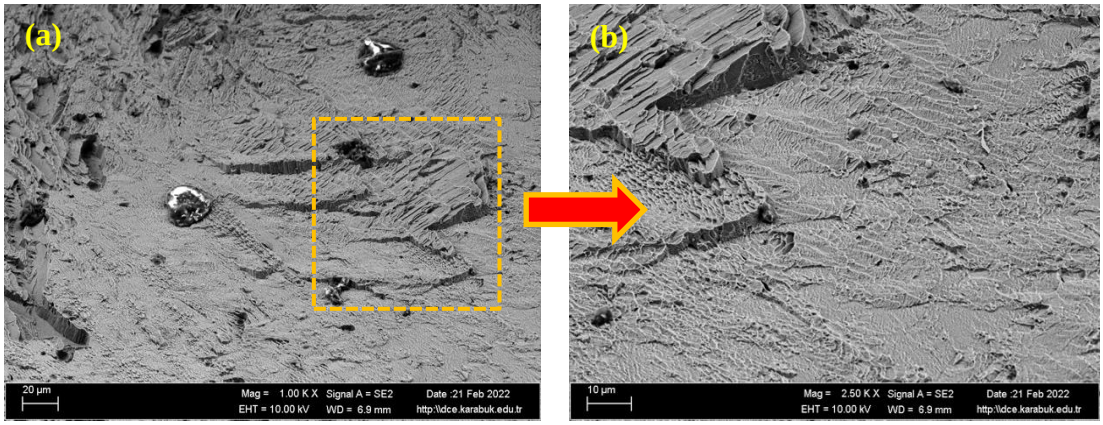

Figure 4.6. Fracture surface of the Cu-Al-Ni SMA after the tensile test (a) Low magnification, (b) High magnification.

Another possibility is that the formation of platelike martensite, the partition of inclusions at grain boundaries, and high elastic anisotropy at grain borders might influence the development of fractures and the strength of material. They can, however, hinder fracture propagation by modifying the propagation route and/or making the crack sufficiently enormous [16, 49, 144-147]. These tendencies may be explained when the fracture is large enough, as seen in **Figure 4.6**, and elastic anisotropy is happening. The crack points have enough stress to cross the grain boundaries, limiting fracture propagation. As a result of accommodating and/or displacing the stress created during the development of the martensite-induced lead, the size of the crack was reduced while maintaining a tiny orientation. Deformation, often known as "cold work," the inclusion of alloying elements, and/or ageing treatment are all viable options for preventing the forming of intergranular fractures.

4.4.3. Shape Memory Effect

The shape memory effect Cu-Al-Ni SMA was shown with a constant applied temperature of 150 °C (below M_f) and a strain of 1.5 %. Other research [68, 132, 148] has observed that the Cu-Al-Ni SMA has a poor strain recovery ratio of 65 % from its original shape. After being unloaded, the specimen was heated to 150 °C (above absolute zero), which resulted in it recovering 65 % of its previous shape. Because of the alloy's shape memory properties, the $\gamma`_1$ and $\beta`_1$ martensite phases, and their morphology, distribution, and volume fraction in the microstructure, this behavior may be explained. According to the thermo-mechanical description, martensite can be found in various distinct microstructures. Internal twinning occurs in the thermal martensite, producing a coherent mirror imitation of the lattice formed across each twin border (special crystallographic planes). The following are some prerequisites for shape memory behavior [149]: for instance, the volume change from austenite to martensite is minimal, and the distortional stresses compared to austenite are generally less than 10 %. In other words, structural change may occur even in the absence of diffusion or flexibility if only very little, coordinated alterations are made in atomic sites. The capacity of martensite to reorganize into a self-accommodating, finely twined structure with very little or no macroscopic strain, as opposed to austenite, is what causes the shape memory effect. Austenite cannot rearrange into this structure. This could take very little, or perhaps no, effort at all to bring about. As a consequence of this, very little strain is normally seen during the transition from austenite to martensite (called shape memory effect). Thermal martensite [150] is the name given to this self-accommodating form. On the other hand, low stress can lead to plastic deformation motion of imperfections such as dislocations, intrinsic twins, and boundary contacts between the martensite phases.

4.5. EFFECT OF DEFORMATION ON

4.5.1. Microstructure of Cu-Al-Ni Shape Memory Alloys

As shown in Figure 4.7 (a-c), the deformation influences on the martensitic phase structure and orientations were studied for Cu-Al-Ni SMAs subjected to three distinct

deformation percentages: 1%, 2%, and 4%. The deformed samples were described using SEM, and their microstructures were analyzed to determine whether the deformation affected the main phases' structure, orientation, or volume fraction.

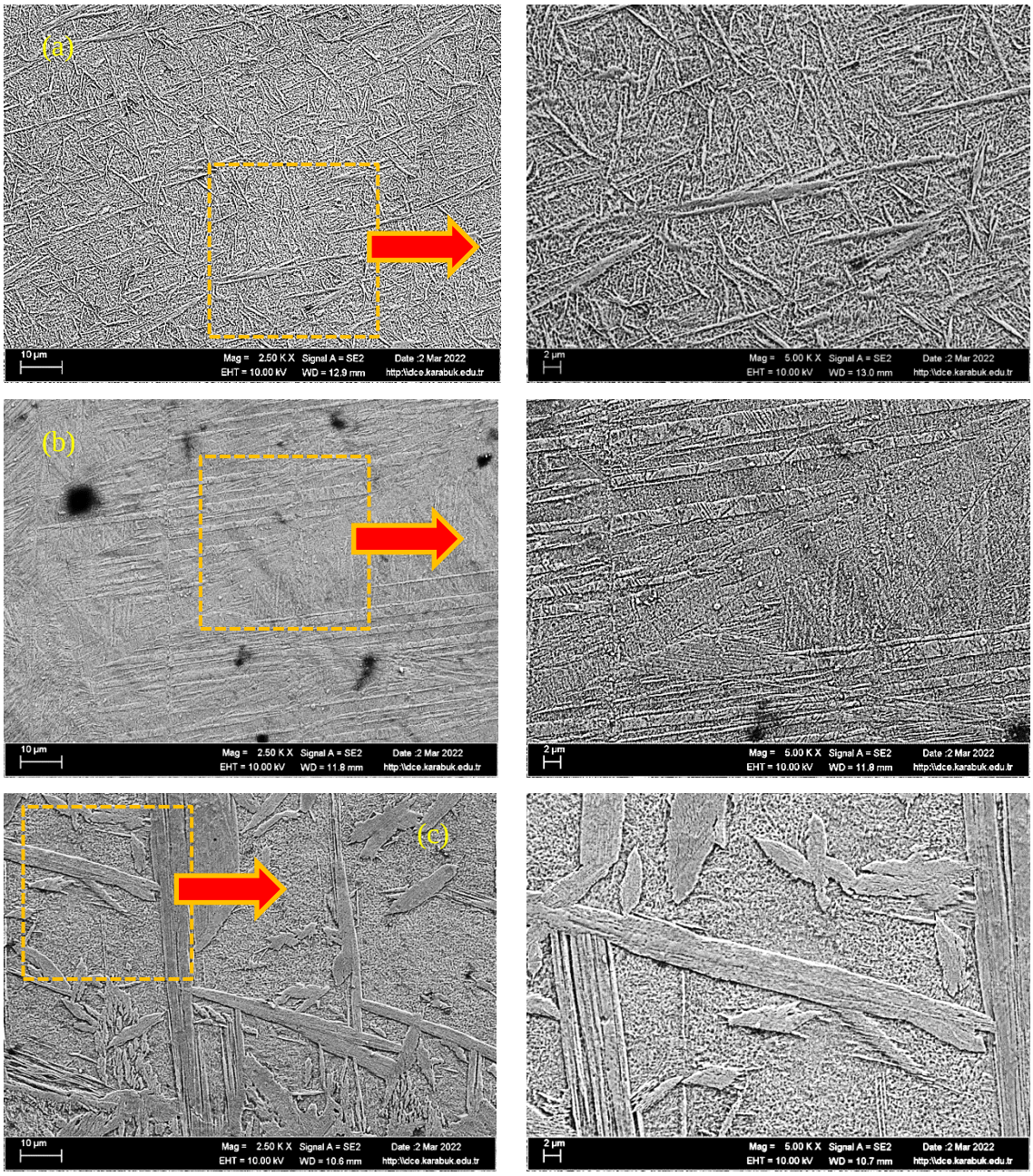

Figure 4.7. Micrographs of Cu-Al-Ni SMAs after different deformation percentages were applied (a) 1%, (b) 2%, and (c) 4%.

Figure 4.7a depicts the sample's microstructure after it was plastically deformed by 1% during the rolling process. It has been demonstrated beyond a reasonable doubt

that coarse versions of the γ'_1 phase martensite are present, in addition to lesser amounts of the β_1' phase martensite with the typical zig-zag shape [22]. In contrast to this, the undeformed sample is composed primarily of β_1' martensite phase with just a trace quantity of γ_1' martensite present (see **Figure 4.1b**). In addition, as shown in **Figure 4.7b**, a larger percentage of the applied deformation results in a thicker γ_1' that is also oriented horizontally along with the direction of the rolling force. This phenomenon may be observed when the rolling force is applied. After applying a further 4 percent of deformation, as shown in **Figure 4.7c**, the thickness of the γ_1' is achieved to be bigger, and the β_1' martensite that is generated between the γ_1' plate-like structures is reduced in terms of size. In addition, one other noticeable morphological shift is the appearance of mechanical twins in the population. It is hypothesized that these identical twins are two intertwined γ_1' martensites. Due to the fact that they are present, we may conclude that the reorientations of martensite plates that occur during deformation are not random [13]. **Figure 4.8(a-c)** displays the EDX analysis findings obtained from the distorted samples.

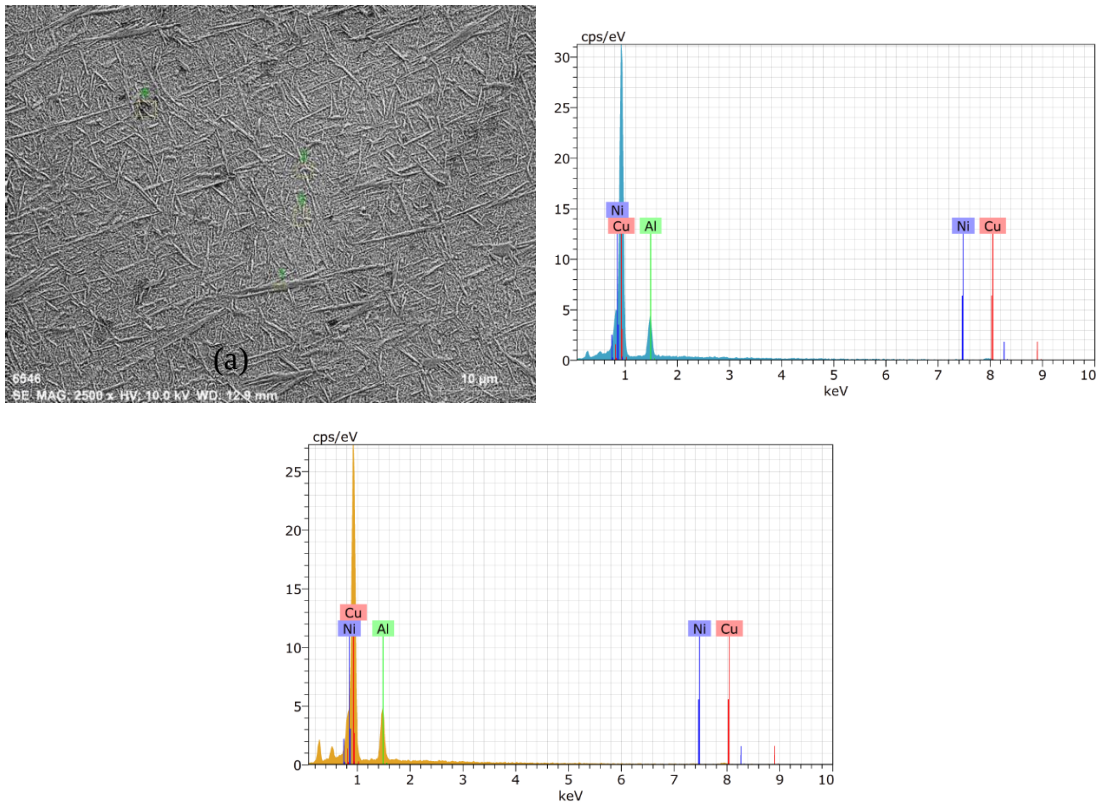

Figure 4.8. EDX spectrums of the Cu-Al-Ni SMAs under different deformation percentages of (a) 1%, (b) 2%, and (c) 4%.

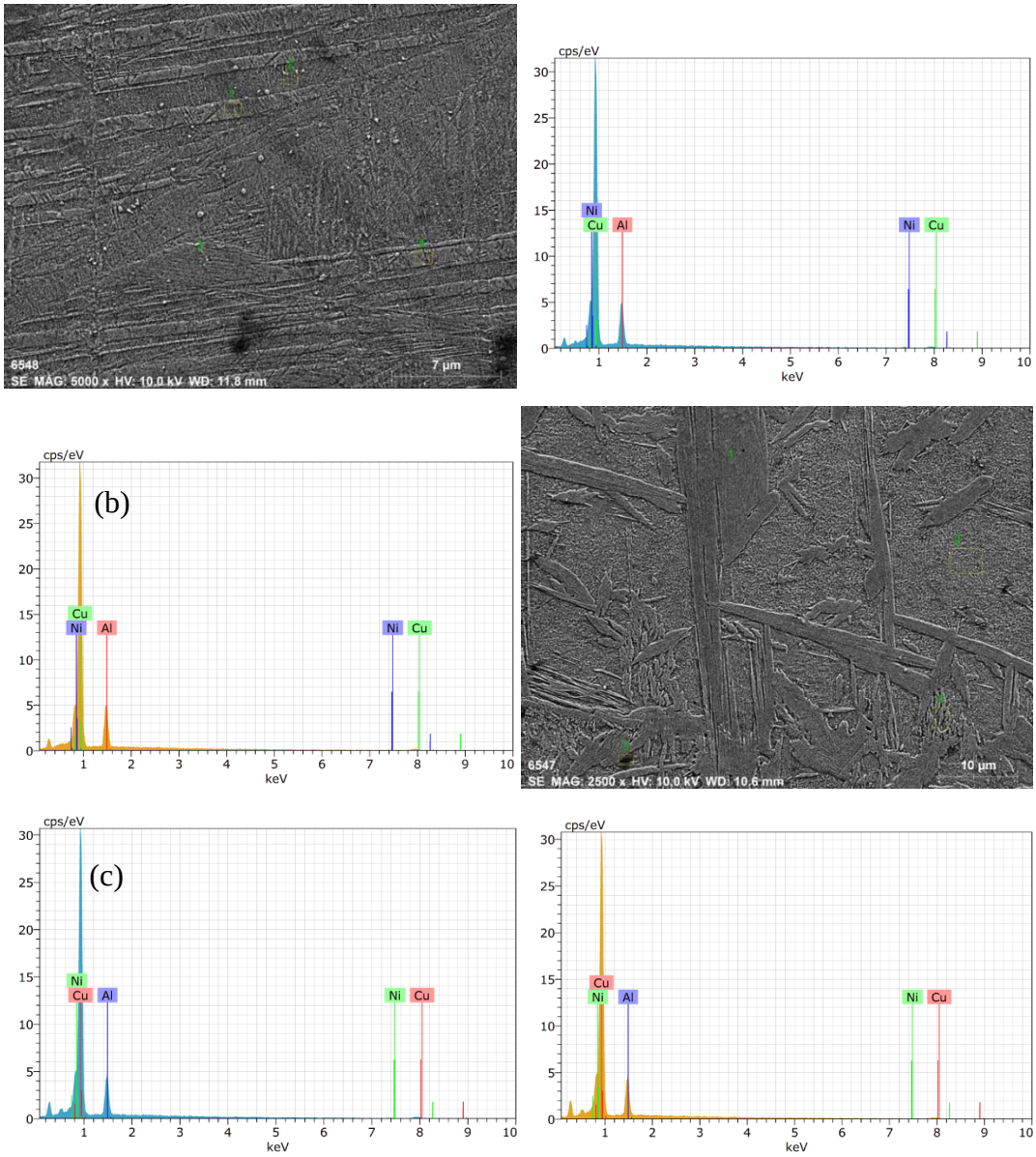

Figure 4.8. (Continued).

Figure 4.9 displays the XRD diffraction patterns of the deformed samples. These patterns were evaluated so that the influence of the applied deformation could be highlighted on the phase existence, characteristics, and intensity. The peak patterns of the distorted microstructures provided conclusive evidence for the presence of two metastable phases, $\gamma`_1$ and $\beta`_1$. Peaks (200), (202), and (1210) all represent the $\gamma`_1$ phase, while the remaining peaks all represent the $\beta`_1$ phase. However, it was seen that following the deformation; there was a considerable change in the patterns; these changes are indicated by moving the peaks and/or raising the intensity, depending on the deformation percentage.

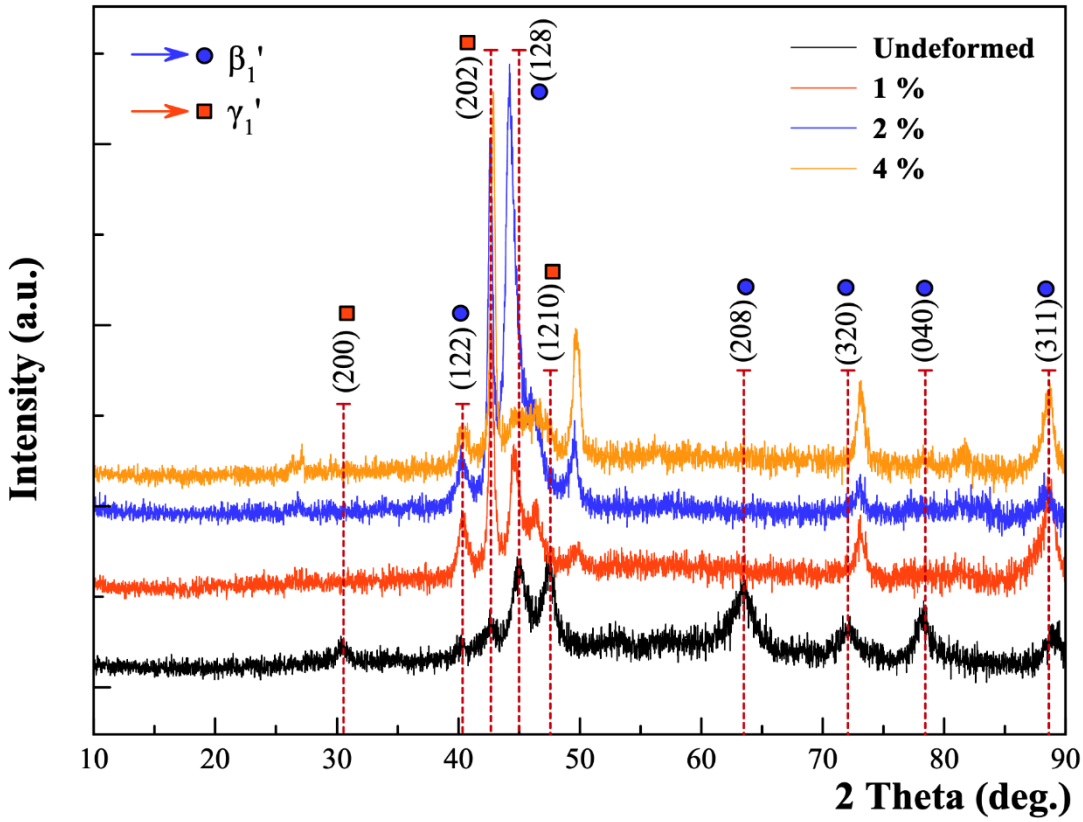

Figure 4.9. X-ray diffractions of the Cu-Al-Ni SMAs under different deformation percentages.

4.5.2. Phase Transformation Temperature

The findings of the differential scanning calorimetry (DSC) performed on deformed Cu-Al-Ni-SMAs under various percentages (1 %, 2 %, and 4 %) for heating and cooling operations are presented in Figure 4.10. The austenite to martensite transformation was analyzed using DSC curves, which allowed the transformation temperatures to be calculated. During the heating process, just one peak was noticed, and then, during the cooling process, the exact opposite of this peak was observed. After deformation was applied, the shapes of the detected peaks changed, and the peaks themselves shifted toward higher transformation temperatures. It is common knowledge that the martensitic transformation is a diffusionless transition that takes place in a crystalline solid between a high transformation temperature phase and a low transformation temperature phase. This transition corresponds to a first-ordered phase structure. After deformation, the DSC graphs in **Figure 4.10** show that the curves of both the heating and cooling processes got narrower. This may be attributed to the

changes in the microstructure of the γ`1 and β`1 phases, as seen in the graphs. The stability of Martensite may also play a significant part in the phenomenon of shifting, which occurred following the deformation of the material. It is also possible to notice that when the percentage of the deformation climbed to 4 %, the temperature of the martensite (both M_s and M_f) reduced to a lower temperature. This occurred directly due to the high-volume fraction of the γ`1 phase.

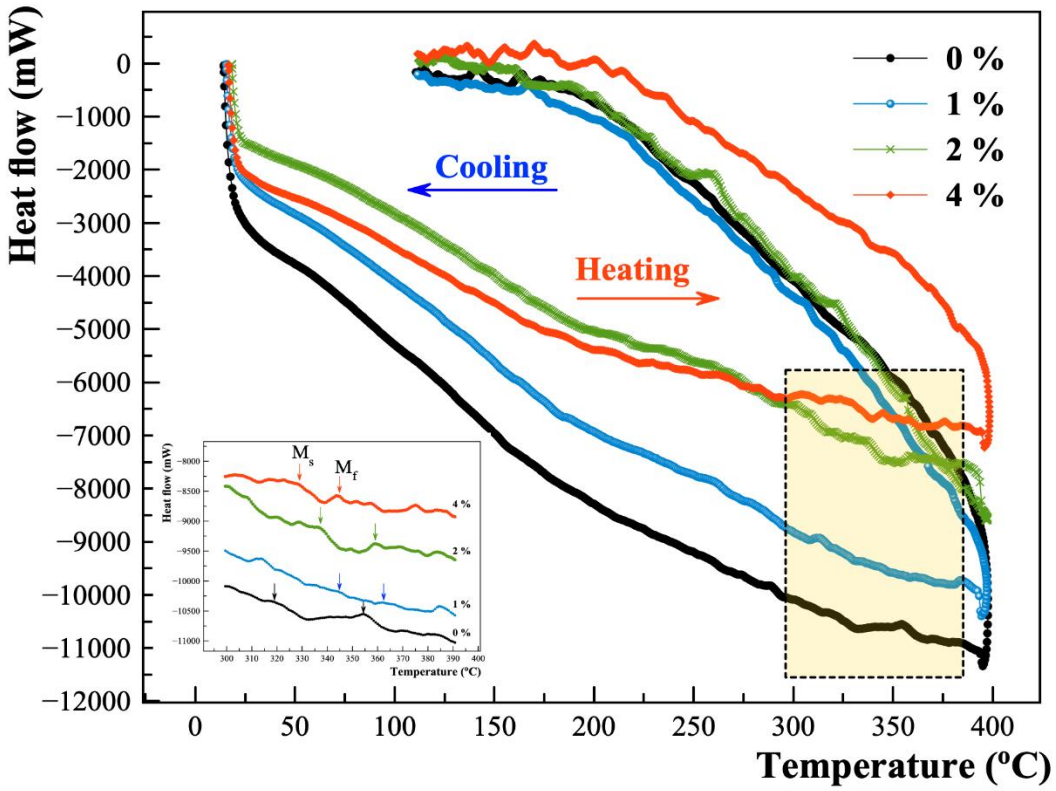

Figure 4. 10Phase transformation curves of the Cu-Al-Ni SMAs under different deformation percentages.

4.5.3. Mechanical Properties of Cu-Al-Ni Shape Memory Alloys

4.5.3.1. Hardness

Using the Vickers Hardness Test Machine, the surface of the specimen is subjected to the hardness test both before and after the deformation process. The loading speed is 65 μm per second, and the loading time is 15 seconds. Other loading parameters, such as the load time, are also specified. The results of hardness tests conducted on Cu-Al-

Ni SMAs before and after the deformation procedure are depicted in Figure 4.11. According to Figure 4.11, the sample taken before the deformation process had the greatest hardness value of 304.6 Hv, while the 4 % deformation showed the lowest hardness value of 247.6 Hv. As a result, the value of the material's hardness fell as the percentage of its deformation increased.

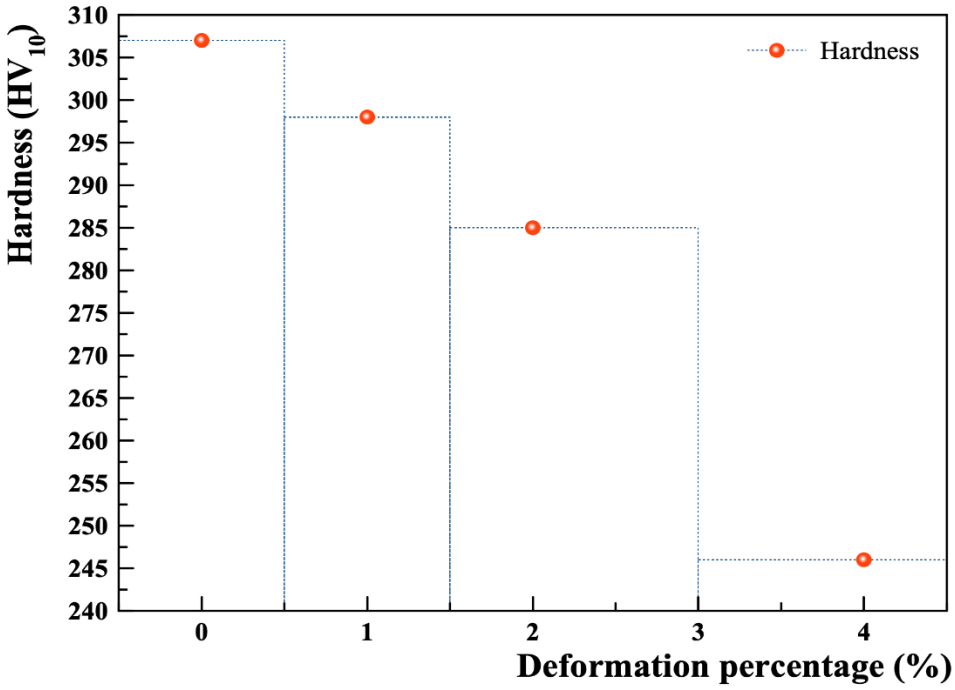

Figure 4.11. Hardness values of the Cu-Al-Ni SMAs under different deformation percentages.

4.5.3.2. Tensile Test

Figure 4.12 illustrates the stress-strain curve produced at room temperature with a continuous strain of 0.1 mm/min with varying percentage deformation. It exhibits a distinct elastic area followed by a linear plastic deformation zone, a classic shape memory alloy property. The induced martensite-martensite deformation area and the direction of the martensite detwinning/variants are primarily responsible for forming subsequent regions in a martensite microstructure. According to Figure 4.12, it can be seen that the tensile stress of Cu-Al-Ni SMAs without deformation displays the lowest value and that when deformation is applied, there is a large rise in the values of the tensile strength owing to the fact that strength hardening occurs that will be able to

hinder the movement of dislocations and thus improve the ductility of brittle Cu-Al-Ni SMAs. The elastic deformation stage, known as region I, is characterized by linear elastic behavior. Region II, the hardening stage, exhibits strain hardening behavior as a result of dislocation structure production during plastic deformation and the subsequent growth of stress-dependent martensite variations. Together, they account for the strain hardening tendency seen at this stage. The surrounding landscape is altered here, particularly in the vicinity of the crack.

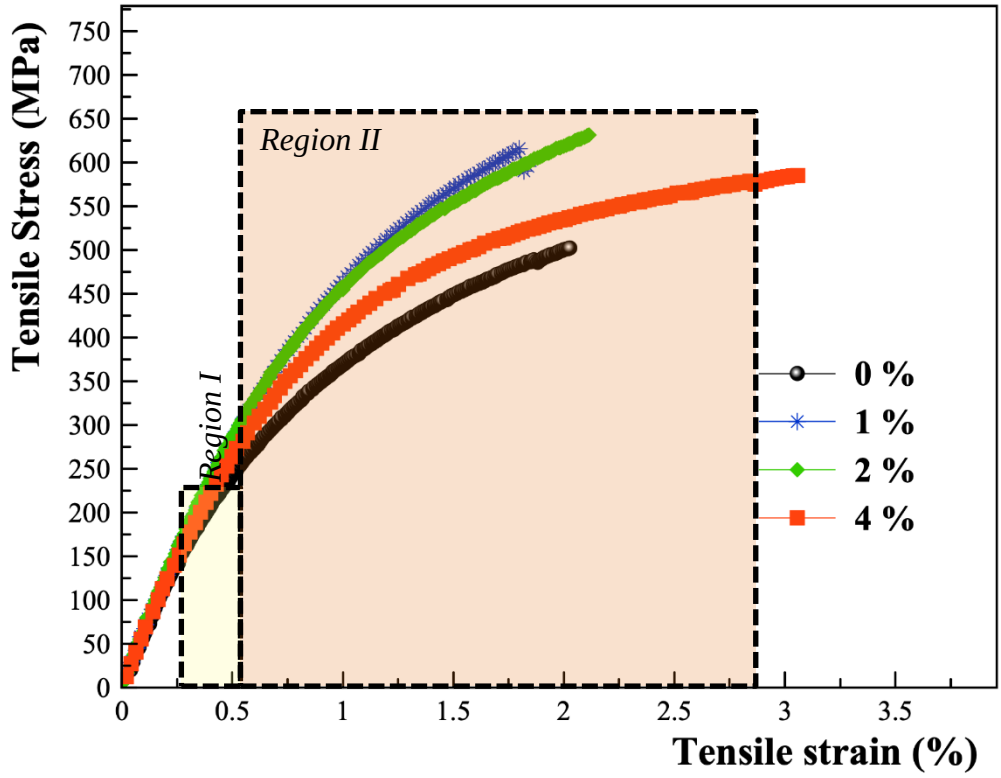

Figure 4.12. Stress-strain curves of the Cu-Al-Ni SMAs under different deformation percentages.

Compression tests were carried out until failure occurred, and subsequent scanning electron microscopy studies of the fracture surfaces were then used to analyse the fracture behaviour of the alloy. Figure 4.13 illustrates the fracture stress and strain values determined by measuring the stress-strain curves. According to the findings, the alloy's fracture undergoes substantial modification due to the deformation process. While samples with 1% and 2% deformation are believed to have better fracture strength than samples that have not been deformed, the fracture strain in this sample has been marginally lowered. To put it another way, the ultimate tensile strength rose

together with the proportion of material deformation applied. In contrast, the undeformed sample does not display ductile fracture after considerable plastic deformation, but the sample that has been deformed by 4 %. **Figure 4.13 (a-c)** illustrates SEM pictures of the fracture surface features of these samples. These images reveal that the deformed samples typically display intergranular fracture characteristics. This is demonstrated by the fact that these images are shown. This is the fracture surface that was created after rolling, and it demonstrates a combination of ductile and brittle fracture. The characteristics include a great number of ductile dimples, voids that point to the ductile failure, and cleavage planes (flat planes with atomic steps that are tiny, suggesting brittle fracture). The sample shown in **Figure** 4.13c has typical ductile failure characteristics, including mixed intergranular and transgranular features. This deformation level corresponds to 4% overall sample volume.

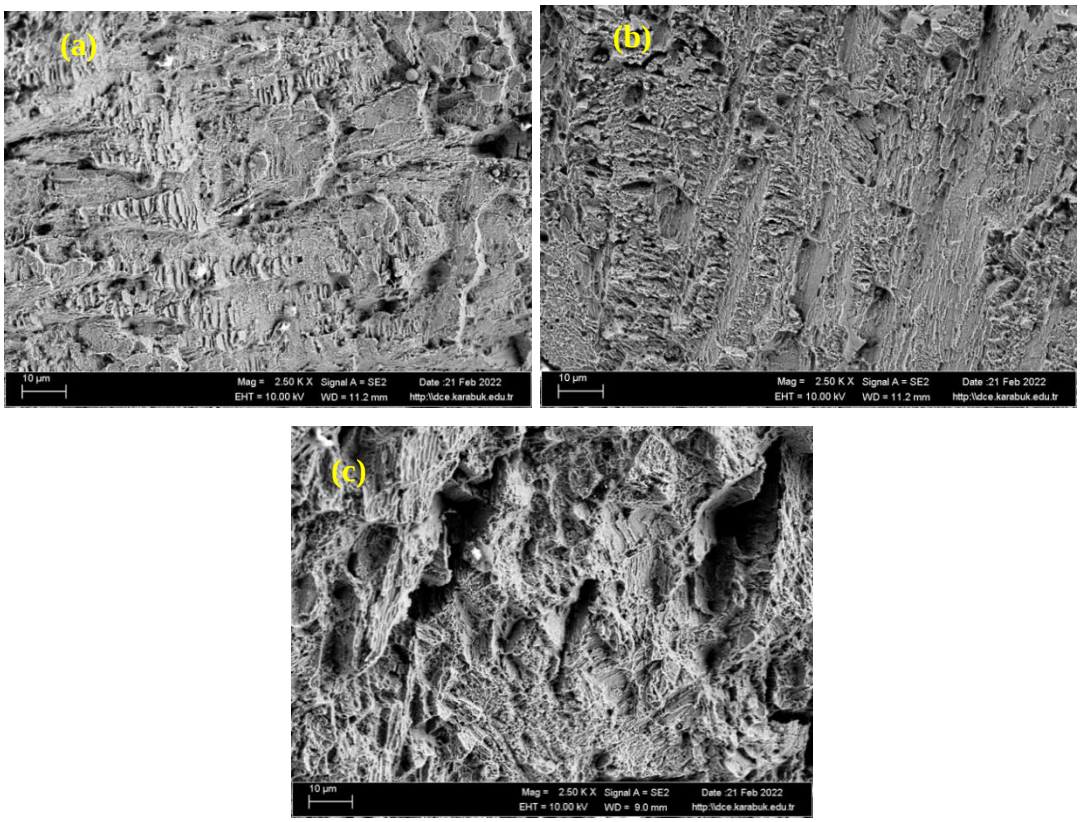

Figure 4.13. Fracture surface area of the Cu-Al-Ni SMAs under different deformation percentages of (a) 1%, (b) 2%, and (c) 4%.

4.5.3.3 Shape Memory Effect

The strain recovery caused by the shape memory of Cu-Al-Ni SMAs was measured by subjecting the material to a tensile test at a temperature higher than M_f. The results of this test were then used to compute the percentage of strain recovery caused by the length mechanism. As seen in Figure 4.14, the consequences of the shape memory changed depending on the degree to which the material was deformed. After being heated to a temperature greater than A_f, the percentages of shape recovery were calculated. These improvements in the strain recovery were linked to the formation and orientation of the $\gamma`_1$ and $\beta`_1$ phases, which were taken about by deformation in the parent phase. This deformation was what brought about these improvements. In addition, the shape recovery percentages were mostly reliant on the amount of the martensitic transformation of the deformed alloys. This could be seen from the peaks of the XRD, which showed a higher intensity when the deformation occurred. It was also found that the sample that underwent a deformation process had a greater value of tensile stress compared to the sample with no deformation process performed on it. According to the findings, the amount of length recovered was proportional to the amount of deformation applied, with a recovery of 94.6 % of the original length achieved when a 2 % of the deformation was applied.

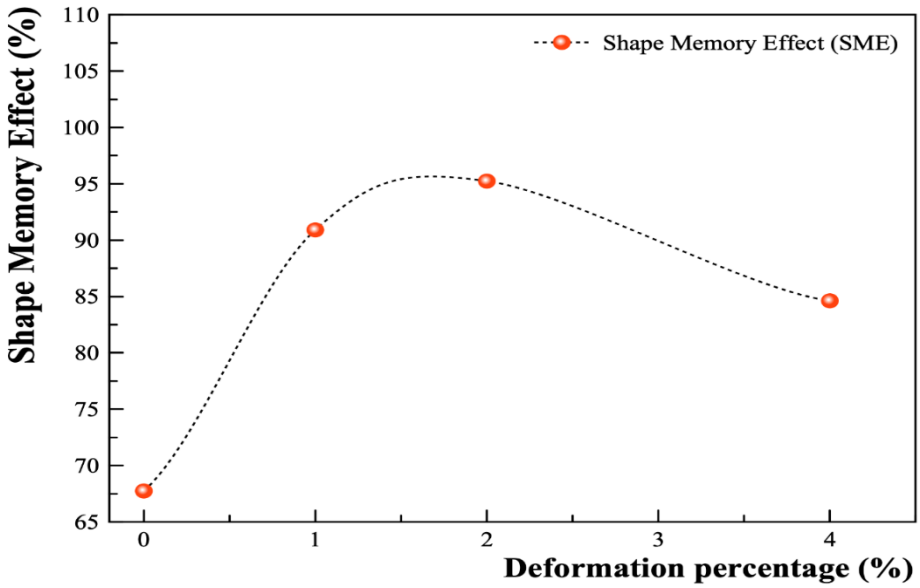

Figure 4.14. Shape memory effects of the Cu-Al-Ni SMAs under different deformation percentage.

CHAPTER 5

CONCLUSIONS AND RECOMMENDATION FOR FUTURE WORKS

5.1. CONCLUSION

From this study of Cu-Al-Ni shape memory alloys under deformation, we may infer the following about their microstructure, mechanical characteristics, and shape memory behaviour's, as follows:

1. According to the findings of the observations, the β_1' and γ_1' martensite phases coexist in the undeformed and deformed states, although at different percentages in each condition. The relative quantities of martensites β_1' and γ_1' can alter because of deformation; the transition of $\beta_1' \rightarrow \gamma_1'$ successive is strengthened as a result of the 4 % deformation. The martensites formed as a result of the deformation have a different shape and develop at new preferred orientations. When the amount of deformation is increased, there is a corresponding rise in the density of reoriented martensite's, formed dislocations and de-twinning structures.

2. The deformation % affected the phase change properties of Cu-Al-Ni SMA, specifically on the temperatures at which the transformation took place. As soon as the deformation loads were applied, the temperatures of the transformation were changed to lower temperatures.

3. Cu–Al–Ni SM alloys may exhibit enhanced ductility and thermomechanical characteristics due to a particular microstructure produced by rolling. In addition, the existence of this sophisticated microstructure does act as a significant barrier to the free movement of martensite plates. Therefore, better

ductility is produced while maintaining appropriate thermomechanical behaviour.

4. The stress-strain and fracture behaviour of the alloy are both influenced by the deformation, which causes significant changes in the mechanical characteristics of the alloy when varying amounts of deformation are applied. When deformed at a percentage of 4 %, the alloy displays intergranular and transgranular characteristics. Despite this, it has a ductile failure behaviour, meaning that it fractures in a combination of intergranular and transgranular ways. In addition, after being distorted at a rate of 2 %, the alloy shows signs of strain hardening. These alterations are brought about by the structure and orientations of the martensite phase.

5. The shape memory effect, acting in concert with the length mechanism, has increased the strain recovery ratio after the deformation has been applied. Under the deformation percentage of 2 %, it was noticed that a remarkable shape recovery of 94.6 percent took place.

5.2. RECOMMENDATION FOR FUTURE WORKS

There are some recommendations for future works, which are as follows:

1. Materials characterizations required for details to taken into consideration through specific equipment's such as transmission electron microscopy or Electron beam selective melting (EBSM).
2. Apply the second type of deformation as hot deformation within certain range of applying loads.
3. Modify the percentage of Al and/or Ni to cover wide range of application, especially for high temperature alloys.

REFERENCES

1. Das, P.P., et al., Advancement in hybrid materials, its applications and future challenges: A review. Materials Today: Proceedings, 2021. **47**: p. 3794-3801.

2. Ghareeb, N. and M. Farhat, Smart materials and structures: State of the art and applications. Nano Res. Appl, 2018. **4**: p. 1-5.

3. Rao, A., A.R. Srinivasa, and J.N. Reddy, Design of shape memory alloy (SMA) actuators. Vol. 3. 2015: Springer.

4. Rao, A., A. Srinivasa, and J. Reddy, Introduction to shape memory alloys, in Design of Shape Memory Alloy (SMA) Actuators. 2015, Springer. p. 1-31.

5. Galindo Quintas, C., Shape Memory Alloys. 2016.

6. DesRoches, R. and B. Smith, Shape memory alloys in seismic resistant design and retrofit: a critical review of their potential and limitations. Journal of earthquake engineering, 2004. **8**(3): p. 415-429.

7. Saud, S.N., E. Hamzah, and T.A.A. Bakar, A review on influence of alloying elements on the microstructure and mechanical properties of Cu-Al-Ni shape memory alloys. Jurnal Teknologi, 2013. **64**(1).

8. Jani, J.M., et al., A review of shape memory alloy research, applications and opportunities. Materials & Design (1980-2015), 2014. **56**: p. 1078-1113.

9. Patil, D. and G. Song, A review of shape memory material's applications in the offshore oil and gas industry. Smart Materials and Structures, 2017. **26**(9): p. 093002.

10. Kong, M., D. Axinte, and W. Voice, Challenges in using waterjet machining of NiTi shape memory alloys: An analysis of controlled-depth milling. Journal of Materials Processing Technology, 2011. **211**(6): p. 959-971.

11. Otsuka, K. and X. Ren, Recent developments in the research of shape memory alloys. Intermetallics, 1999. **7**(5): p. 511-528.

12. Rondelli, G. and B. Vicentini, Localized corrosion behaviour in simulated human body fluids of commercial Ni–Ti orthodontic wires. Biomaterials, 1999. **20**(8): p. 785-792.

13. Rasheed, M.S., et al., Analysis of influence of micro-EDM parameters on MRR, TWR and Ra in machining Ni-Ti shape memory alloy. International Journal of Recent Technology and Engineering, 2012. **1**(4): p. 32-37.

14. Al-Humairi, S.N.S., Cu-based shape memory alloys: modified structures and their related properties. Recent Advancements in the Metallurgical Engineering and Electrodeposition, 2020. **25**.

15. Kannan, T.D.B., P. Sathiya, and T. Ramesh, 23 Laser Welding of NiTinol Shape Memory Alloy.

16. Miyazaki, S., et al., The fracture of Cu–Al–Ni shape memory alloy. Transactions of the Japan Institute of Metals, 1981. **22**(4): p. 244-252.

17. Lojen, G., et al., Microstructure of rapidly solidified Cu–Al–Ni shape memory alloy ribbons. Journal of Materials Processing Technology, 2005. **162**: p. 220-229.

18. Lecroisey, F. and A. Pineau, Martensitic transformations induced by plastic deformation in the Fe-Ni-Cr-C system. Metallurgical and Materials Transactions B, 1972. **3**(2): p. 391-400.

19. Sarı, U. and T. Kırındı, Effects of deformation on microstructure and mechanical properties of a Cu–Al–Ni shape memory alloy. Materials Characterization, 2008. **59**(7): p. 920-929.

20. Schroeder, T. and C. Wayman, The formation of martensite and the mechanism of the shape memory effect in single crystals of Cu-Zn alloys. Acta Metallurgica, 1977. **25**(12): p. 1375-1391.

21. Juan, J.S., M.L. Nó, and C.A. Schuh, Nanoscale shape-memory alloys for ultrahigh mechanical damping. Nature nanotechnology, 2009. **4**(7): p. 415-419.

22. Sapozhnikov, K., et al., Motion of dislocations and interfaces during deformation of martensitic Cu–Al–Ni crystals. Acta materialia, 2000. **48**(5): p. 1141-1151.

23. Saud, S.N., et al., Thermal aging behavior in Cu–Al–Ni–xCo shape memory alloys. Journal of Thermal Analysis and Calorimetry, 2015. **119**(2): p. 1273-1284.

24. Dasgupta, R., A look into Cu-based shape memory alloys: Present scenario and future prospects. Journal of Materials Research, 2014. **29**(16): p. 1681-1698.

25. Hartl, D.J. and D.C. Lagoudas. Simultaneous transformation and plastic deformation in shape memory alloys. in Behavior and Mechanics of Multifunctional and Composite Materials 2008. 2008. International Society for Optics and Photonics.

26. Agrawal, A. and R.K. Dube, Methods of fabricating Cu-Al-Ni shape memory alloys. Journal of Alloys and Compounds, 2018.

27. Otsuka, K. and C.M. Wayman, Shape memory materials. 1999: Cambridge university press.

28. Otsuka, K.a.X.R., Martensitic transformations in nonferrous shape memory alloys. Materials Science and Engineering: A, 1999. **273–275(0)**: p. 89-105.

29. Pelegrina, J., A. Yawny, and M. Sade, Diffusive Phenomena and the Austenite/Martensite Relative Stability in Cu-Based Shape-Memory Alloys. Shape Memory and Superelasticity, 2018. **4**(1): p. 48-60.

30. Rodríguez-Aseguinolaza, J., et al., Temperature memory effect in Cu–Al–Ni shape memory alloys studied by adiabatic calorimetry. Acta Materialia, 2008. **56**(15): p. 3711-3722.

31. Ruiz-Larrea, I., et al., The specific heat of Cu–Al–Ni shape memory alloys. Materials Science and Engineering: A, 2006. **438-440**: p. 779-781.

32. Mukunthan, K. and L. Brown, Preparation and properties of fine grain β-CuAlNi strain-memory alloys. Metallurgical Transactions A, 1988. **19**(12): p. 2921-2929.

33. Musolff, A. and H. Sahota, Phase transitions in the shape memory alloy CuAlNi. Continuum Mechanics and Thermodynamics, 2004. **16**(6): p. 539-549.

34. Zhang, X., L. Brinson, and Q.-P. Sun, The variant selection criteria in single-crystal CuAlNi shape memory alloys. Smart materials and structures, 2000. **9**(5): p. 571.

35. Lagoudas, D.C., Shape Memory Alloys: Modeling and Engineering Applications. 2008: Springer.

36. Saburi, T., et al., The shape memory mechanism in 18R martensitic alloys. Acta Metallurgica, 1980. **28**(1): p. 15-32.

37. Alkan, S., et al., Transformation stress of shape memory alloy CuZnAl: Non-Schmid behavior. Acta Materialia, 2018. **149**: p. 220-234.

38. Carpinteri, A., et al., Mechanical behaviour and phase transition mechanisms of a shape memory alloy by means of a novel analytical model. acta mechanica et automatica, 2018. **12**(2): p. 105-108.

39. D.C.Lagoudas, Shape Memory Alloys and Engineering Applications. 2008: Springer, New York.

40. Kumar, P. and D. Lagoudas, Introduction to shape memory alloys. 2008: Springer.

41. Saud, S., et al., Influence of Ti additions on the martensitic phase transformation and mechanical properties of Cu–Al–Ni shape memory alloys. Journal of Thermal Analysis and Calorimetry, 2014: p. 1-12.

42. Kuwano, N.a.C.M.W., Some Effects of Parent Phase Aging on the Martensitic Transformation in A Cu-Al-Ni Shape Memory Alloy. Metallurgical transactions. A, Physical Metallurgy and Materials Science, 1984. **15 A(4)**: p. 621-626.

43. Badawy, W., M. El-Rabiei, and H. Nady, Synergistic effects of alloying elements in Cu-ternary alloys in chloride solutions. Electrochimica Acta, 2014. **120**: p. 39-45.

44. Waitz, T., et al., Size effects on martensitic phase transformations in nanocrystalline NiTi shape memory alloys. Materials Science and Technology, 2008. **24**(8): p. 934-940.

45. Dutkiewicz, J., T. Czeppe, and J. Morgiel, Effect of titanium on structure and martensic transformation in rapidly solidified Cu–Al–Ni–Mn–Ti alloys. Materials Science and Engineering: A, 1999. **273**: p. 703-707.

46. Tadaki, T., Cu-based shape memory alloys. Shape memory materials, 1998: p. 97-116.

47. Miyazaki, S., T. Kawai, and K. Otsuka, Study of fracture in Cu-Al-Ni shape memory bicrystals. Le Journal de Physique Colloques, 1982. **43**(C4): p. C4-813-C4-818.

48. Horikawa, H., et al., Orientation dependence of β1 → β1′ stress-induced martensitic transformation in a Cu-AI-Ni alloy. Metallurgical Transactions A, 1988. **19**(4): p. 915-923.

49. Otsuka, K., H. Sakamoto, and K. Shimizu, Successive stress-induced martensitic transformations and associated transformation pseudoelasticity in Cu-Al-Ni alloys. Acta Metallurgica, 1979. **27**(4): p. 585-601.

50. Eisenwasser, J. and L. Brown, Pseudoelasticity and the strain-memory effect in Cu-Zn-Sn alloys. Metallurgical Transactions, 1972. **3**(6): p. 1359-1363.

51. Kennon, N., D. Dunne, and L. Middleton, Aging effects in copper-based shape memory alloys. Metallurgical Transactions A, 1982. **13**(4): p. 551-555.

52. DUNNE, N.F.K.a.D.P., SHAPE STRAINS ASSOCIATED WITH THERMALLY-INDUCED AND STRESS-INDUCED

MARTENSITE IN A Cu-Al-Ni SHAPE MEMORY ALLOY. Acta Metall, 1982. **30**: p. 429-435.

53. Zhang Xiangyang, S.Q., Yu Shouwen, A non-invariant plane model for the interface in CuAlNi single crystal shape memory alloys. Journal of the Mechanics and Physics of Solids, 2000. **48**: p. 2163–2182.

54. Nó, M.L., D. Caillard, and J. San Juan, A TEM study of martensite habit planes and orientation relationships in Cu–Al–Ni shape memory alloys using a fast Δg-based method. Acta Materialia, 2009. **57**(4): p. 1004-1014.

55. Qiao, L., et al., Nonlocal Superelastic Model of Size-Dependent Hardening and Dissipation in Single Crystal Cu-Al-Ni Shape Memory Alloys. Physical Review Letters, 2011. **106**(8).

56. Xu, J.W., Effects of Gd addition on microstructure and shape memory effect of Cu–Zn–Al alloy. Journal of Alloys and Compounds, 2008. **448**(1-2): p. 331-335.

57. Castro, M.L.a.R.R., Isothermal decomposition of some β Cu-Zn-Al alloys with e/a=1.48. Materials Science and Engineering A 1999. **273-275:**: p. 577-580.

58. Agrawal, A. and R.K. Dube, Methods of fabricating Cu-Al-Ni shape memory alloys. Journal of Alloys and Compounds, 2018. **750**: p. 235-247.

59. Saud, S.N., et al., Effects of Quenching Media on Phase Transformation Characteristics and Hardness of Cu-Al-Ni-Co Shape Memory Alloys. Journal of Materials Engineering and Performance, 2015. **24**(4): p. 1522-1530.

60. Gustmann, T., et al., Properties of Cu-based shape-memory alloys prepared by selective laser melting. Shape Memory and Superelasticity, 2017. **3**(1): p. 24-36.

61. Gera, D.B., et al., The Influence of Sintering Parameters in the Microstructure and Mechanical Properties of a Cu–Al–Ni–Mn–Zr Shape Memory Alloy. Advanced Engineering Materials, 2018. **20**(10): p. 1800372.

62. Velmurugan, C. and V. Senthilkumar, The effect of Cu addition on the morphological, structural and mechanical characteristics of nanocrystalline NiTi shape memory alloys. Journal of Alloys and Compounds, 2018. **767**: p. 944-954.

63. Li, D.-y., et al., Superelasticity of Cu–Ni–Al shape-memory fibers prepared by melt extraction technique. International Journal of Minerals, Metallurgy, and Materials, 2016. **23**(8): p. 928-933.

64. Otsuka, K., A. Saxena, J. Deng and Xiaobing Ren Mechanism of the shape memory effect in martensitic alloys: an assessment. Philosophical Magazine, 2011. **91**(36): p. 4514-4535.

65. Bayram, Ü. and N. Maraşlı, Thermal conductivity and electrical resistivity dependences on growth rate in the directionally solidified Al–Cu–Ni eutectic alloy. Journal of Alloys and Compounds, 2018. **753**: p. 695-702.

66. Braga, F.d.O., et al., Martensitic Transformation Under Compression of a Plasma Processed Polycrystalline Shape Memory CuAlNi Alloy. Materials Research, 2017. **20**(6): p. 1579-1592.

67. Z.G. Wei, H.Y.P., D.Z. Yang, C.Y. Chung, J.K.L. Lai, Reverse transformations in CuA1NiMnTi alloy at elevated temperatures. Acta Materialia, 1996. **44**(3): p. 1189-1199.

68. Sampath, V., Studies on the effect of grain refinement and thermal processing on shape memory characteristics of Cu–Al–Ni alloys. Smart Materials and Structures, 2005. **14**(5): p. S253-S260.

69. Y. Itsumi, Y.M., T. Takashima, Kazuhito Kamei, Kazuko Sugimoto, The Effects of Ageing on the Martensitic Transformation Temperature in Cu-Al-Ni-Mn-Ti Shape Memory Alloys. Advanced Materials Research, 1991. **56-58**: p. 469-474.

70. Karagoz, Z. and C.A. Canbay, Relationship between transformation temperatures and alloying elements in Cu–Al–Ni shape memory alloys. Journal of Thermal Analysis and Calorimetry, 2013. **114**(3): p. 1069-1074.

71. Chang, S.H., Influence of chemical composition on the damping characteristics of Cu–Al–Ni shape memory alloys. Materials Chemistry and Physics, 2011. **125**(3): p. 358-363.

72. Recarte, V., et al., Dependence of the martensitic transformation characteristics on concentration in Cu–Al–Ni shape memory alloys. Materials Science and Engineering: A, 1999. **273**: p. 380-384.

73. Recarte, V., et al., Study by resonant ultrasound spectroscopy of the elastic constants of the β phase in Cu□Al□Ni shape memory alloys. Materials Science and Engineering: A, 2004. **370**(1-2): p. 488-491.

74. Recarte, V., et al., Vibrational and magnetic contributions to the entropy change associated with the martensitic transformation of Ni-Fe-Ga ferromagnetic shape memory alloys. J Phys Condens Matter, 2010. **22**(41): p. 416001.

75. Sugimoto, K., et al., Grain-refinement and the related phenomena in quaternary Cu-Al-Ni-Ti shape memory alloys. Le Journal de Physique Colloques, 1982. **43**(C4): p. C4-761-C4-766.

76. C.M.Wayman, J.S.L.a., grain refinement of a Cu-Al-Ni shape memory alloys by Ti and Zr additions. transactions of Japan institute of metals, 1986. **27**(8): p. 584 -591.

77. Saud, S.N., et al., Influence of tin additions on the phase-transformation characteristics of mechanical alloyed Cu-Al-Ni shape-memory alloy. Metallurgical and Materials Transactions A, 2016. **47**(10): p. 5242-5255.

78. Bhattacharya B, B.A.a.B.M.K., Influence of minor additions on characteristics of Cu–Al–Ni alloy", Mater. Sci. Technol. 9 654–65, (1993). Mater. Sci. Technol, 1993. **9**: p. 654–658.

79. Chen, C. and T. Liu, Phase transformations in a Cu-14.2 Al-7.8 Ni alloy. Metallurgical and Materials Transactions A, 2003. **34**(3): p. 503-509.

80. Duerig, T.W., Engineering Aspects of Shape Memory Alloys. 1990: Butterworth-Heinemann.

81. Chentouf, S.M., et al., Microstructural and thermodynamic study of hypoeutectoidal Cu–Al–Ni shape memory alloys. Journal of Alloys and Compounds, 2009. **470**(1-2): p. 507-514.

82. V. Recarte, I.H., J. Herreros, M.L. Nó, J.San Juan, Precipitation of the stable phases in Cu-Al-Ni shape memory alloys. Scripta Materialia, 1996. **34**: p. 255-260.

83. Sutou, Y., et al., Characteristics of Cu–Al–Mn-based shape memory alloys and their applications. Materials Science and Engineering: A, 2004. **378**(1-2): p. 278-282.

84. Sutou, Y., et al., Effect of grain size and texture on pseudoelasticity in Cu–Al–Mn-based shape memory wire. Acta Materialia, 2005. **53**(15): p. 4121-4133.

85. Sutou, Y., R. Kainuma, and K. Ishida, Effect of alloying elements on the shape memory properties of ductile Cu–Al–Mn alloys. Materials Science and Engineering: A, 1999. **273**: p. 375-379.

86. Sutou, Y., et al., Effects of grain size and texture on damping properties of Cu–Al–Mn-based shape memory alloys. Materials Science and Engineering: A, 2006. **438**: p. 743-746.

87. Haberkorn, N., et al., Bulk-like behavior in the temperature driven martensitic transformation of Cu–Zn–Al thin films with 2H structure. Journal of alloys and compounds, 2014. **591**: p. 263-267.

88. Fricoteaux, P. and C. Rousse, Nanowires of Cu–Zn and Cu–Zn–Al shape memory alloys elaborated via electrodeposition in ionic liquid. Journal of Electroanalytical Chemistry, 2014. **733**: p. 53-59.

89. LIU, H.-x., N.-c. SI, and G.-f. XU, Influence of process factors on shape memory effect of CuZnAl alloys. Transactions of Nonferrous Metals Society of China, 2006. **16**(6): p. 1402-1409.

90. Kim, J., et al., Microstructure and properties of grain-refined Cu-Zn-Al-X shape memory alloys. Journal of materials science letters, 1990. **9**(4): p. 463-465.

91. Alaneme, K.K. and S. Umar, Mechanical behaviour and damping properties of Ni modified Cu–Zn–Al shape memory alloys. Journal of Science: Advanced Materials and Devices, 2018. **3**(3): p. 371-379.

92. Iacoviello, F., et al., Grain size and loading conditions influence on fatigue crack propagation in a Cu-Zn-Al shape memory alloy. International journal of fatigue, 2018. **115**: p. 27-34.

93. Zhang, D., et al., Selective Hydrogenation of Maleic Anhydride to Tetrahydrofuran over Cu− Zn− M (M= Al, Ti, Zr) Catalysts Using Ethanol As a Solvent. Industrial & engineering chemistry research, 2009. **48**(24): p. 11220-11224.

94. Chentouf, S., et al., Ageing study of Cu–Al–Be hypoeutectoid shape memory alloy. Materials characterization, 2010. **61**(11): p. 1187-1193.

95. López-Ferreño, I., et al., Stress-assisted atomic diffusion in metastable austenite D03 phase of Cu-Al-Be shape memory alloys. Scripta Materialia, 2016. **124**: p. 155-159.

96. Montecinos, S. and S. Simison, Influence of the microstructure on the corrosion behaviour of a shape memory Cu–Al–Be alloy in a marine environment. Applied Surface Science, 2011. **257**(7): p. 2737-2744.

97. Saint-Sulpice, L., S. Arbab-Chirani, and S. Calloch, Thermomechanical cyclic behavior modeling of Cu-Al-Be SMA materials and structures. International Journal of Solids and Structures, 2012. **49**(9): p. 1088-1102.

98. Montecinos, S. and A. Cuniberti, Martensitic transformation and grain size in a Cu-Al-Be alloy. Procedia Materials Science, 2012. **1**: p. 149-155.

99. Saud, S.N., et al., Influence of Ti additions on the martensitic phase transformation and mechanical properties of Cu–Al–Ni shape memory alloys. Journal of Thermal Analysis and Calorimetry, 2014. **118**(1): p. 111-122.

100. Peltier, L., et al., Production and mechanical properties of Cu-Al-Ni-Be shape memory alloy thin ribbons using a cold co-rolled process. Shape Memory and Superelasticity, 2021. **7**(2): p. 344-352.

101. Hodgson, D., Wu, MH, Biermann, RJ, Metals Handbook. ASM International, Ohio, 1990. **2**: p. 897.

102. Gall, K., et al., Thermomechanics of the shape memory effect in polymers for biomedical applications. Journal of Biomedical Materials Research Part A, 2005. **73**(3): p. 339-348.

103. Stöckel, D., The shape memory effect: phenomenon, alloys, applications. 报告 (2000 年), NDC, Nitinol Devices & Components 公司, 美国加利福尼亚州 Fremont, www. nitinol-europe. com/pdfs/smemory. pdf (2007 年 12 月 24 日浏览), 2000.

104. Leo, D.J., et al. Vehicular applications of smart material systems. in 5th Annual International Symposium on Smart Structures and Materials. 1998. International Society for Optics and Photonics.

105. Stoeckel, D., Shape memory actuators for automotive applications. Materials & Design, 1990. **11**(6): p. 302-307.

106. Wilkes, K.E. and P.K. Liaw, The fatigue behavior of shape-memory alloys. JOM, 2000. **52**(10): p. 45-51.

107. Hornbogen, E., Review Thermo-mechanical fatigue of shape memory alloys. Journal of materials science, 2004. **39**(2): p. 385-399.

108. Widdle, R.D., et al., High stiffness shape memory alloy actuated aerostructure. 2013, Google Patents.

109. Mani, R., D.C. Lagoudas, and O.K. Rediniotis. MEMS-based active skin for turbulent drag reduction. in Smart Structures and Materials. 2003. International Society for Optics and Photonics.

110. Tawfik, M., J.-J. Ro, and C. Mei, Thermal post-buckling and aeroelastic behaviour of shape memory alloy reinforced plates. Smart Materials and Structures, 2002. **11**(2): p. 297.

111. Furuya, Y. and H. Shimada, Shape memory actuators for robotic applications. Materials & Design, 1991. **12**(1): p. 21-28.

112. Sreekumar, M., et al., Critical review of current trends in shape memory alloy actuators for intelligent robots. Industrial Robot: An International Journal, 2007. **34**(4): p. 285-294.

113. Wu, M.H. and L. Schetky. Industrial applications for shape memory alloys. in Proceedings of the International Conference on Shape Memory and Superelastic Technologies, Pacific Grove, California. 2000.

114. Russell, S.M., SMST-2000: Proceedings of the International Conference on Shape Memory and Superelastic Technologies. 2001: SMST, the International Organization on Shape Memory and Superelastic Technology.

115. Duerig, T.W., K. Melton, and D. Stöckel, Engineering aspects of shape memory alloys. 2013: Butterworth-heinemann.

116. Song, G., N. Ma, and H.-N. Li, Applications of shape memory alloys in civil structures. Engineering structures, 2006. **28**(9): p. 1266-1274.

117. Hartl, D.J. and D.C. Lagoudas, Aerospace applications of shape memory alloys. Proceedings of the Institution of Mechanical Engineers, Part G: Journal of Aerospace Engineering, 2007. **221**(4): p. 535-552.

118. Jani, J.M., M. Leary, and A. Subic. Shape memory alloys in automotive applications. in Applied Mechanics and Materials. 2014. Trans Tech Publ.

119. Sohn, J.W., G.-W. Kim, and S.-B. Choi, A state-of-the-art review on robots and medical devices using smart fluids and shape memory alloys. Applied Sciences, 2018. **8**(10): p. 1928.

120. Machado, L. and M. Savi, Medical applications of shape memory alloys. Brazilian journal of medical and biological research, 2003. **36**(6): p. 683-691.

121. Obradó, E., L. Manosa, and A. Planes, Stability of the bcc phase of Cu-Al-Mn shape-memory alloys. Physical Review B, 1997. **56**(1): p. 20.

122. Saud, S., et al., Thermal aging behavior in Cu–Al–Ni–xCo shape memory alloys. Journal of Thermal Analysis and Calorimetry, 2015. **119**(2): p. 1273-1284.

123. Bergeon, N., G. Guenin, and C. Esnouf, Study of the Faults Stackings in the γ(f.c.c.)-ε(h.c.p.) Martensitic Transformation. J. Phys. IV France, 1997. **07**(C5): p. C5-125-C5-130.

124. Putaux, J.L. and J.P. Chevalier, HREM study of self-accommodated thermal ε-martensite in an Fe□Mn□Si□Cr□Ni shape memory alloy. Acta Materialia, 1996. **44**(4): p. 1701-1716.

125. Eskil, M. and N. Kayali, X-ray analysis of some shape memory CuZnAl alloys due to the cooling rate effect. Materials Letters, 2006. **60**(5): p. 630-634.

126. Saburi, T. and C.M. Wayman, Crystallographic similarities in shape memory martensites. Acta Metallurgica, 1979. **27**(6): p. 979-995.

127. Yildirim Aydogdu, A.A., Osman Adiguzel, Self-accommodating martensite plate variants in shape memory CuAlNi alloys. Journal of Materials Processing Technology, 2002. **123**: p. 498-500.

128. Friend, C.M., The effect of aluminium content on the martensite phase stabilities in metastable CuAlNi alloys. Scripta Metallurgica, 1989. **23**(10): p. 1817-1820.

129. Nishiyama, Z., M.E. Fine, and C.M. Wayman, Martensitic transformation. 1978: Academic Press.

130. M. Miki, Y.O., Y. Hiramatsu effects of B and Cr additions on the grain refinement and ductility of a Cu-14Al-3Ni shape memory alloy. Nippon Kinzoku Gakkai-si, 1987. **51**(9): p. 815-823.

131. D. W. Roh, J.W.K., T. J. Cho, Y. G. Kim, Tensile properties and microstructure of microalloyed Cu-A1-Ni-X shape memory alloys. Materials Science and Engineering: A, 1991. **136**: p. 17-23.

132. Morris, M.A., Microstructural Influence on Ductility and Shape Memory Effect of some Modified Cu.Ni.Ai Alloys. Scripta Metallugica, 1991. **25**: p. 1409-1414.

133. Morris, M.A.a.S.G., Effect of heat treatment and thermal cycling on transformation temperatures of ductile Cu-Al-Ni-Mn-B alloys. Scripta Metallurgica et Materiala, 1992. **26(11)**: p. 1663-1668.

134. M. O. LAI, L.L., W. H. LEE, Influence of heat treatment on properties of copper-based shape-memory alloy. Journal of Materials Science, 1996. **31**: p. 1537-1543.

135. F. Dagdelen, T.G., A. Aydogdu, Y. Aydogdu, O. Adigu¨zel, Effects of thermal treatments on transformation behaviour in shape memory Cu–Al–Ni alloys. Materials Letters, 2003. **57**: p. 1079-1085.

136. Fernández, J., et al., Thermal stability of the martensitic transformation of Cu–Al–Ni–Mn–Ti. Materials Science and Engineering: A, 2006. **438-440**: p. 723-725.

137. Sutou, Y., et al., Effects of grain size and texture on damping properties of Cu–Al–Mn-based shape memory alloys. Materials Science and Engineering: A, 2006. **438-440**: p. 743-746.

138. Mallik, U.S. and V. Sampath, Influence of aluminum and manganese concentration on the shape memory characteristics of Cu–Al–Mn shape memory alloys. Journal of Alloys and Compounds, 2008. **459** (1-2): p. 142-147.

139. Sakamoto, H. and K.i. Shimizu, Effect of Heat Treatments on Thermally Formed Martensite Phases in Monocrystalline Cu–Al–Ni Shape Memory Alloy. ISIJ International, 1989. **29**(5): p. 395-404.

140. HUANG, W.M., et al., Behaviour of Young's Modulus in Shape Memory Alloys upon Mechanical Loading. Mater Sci ISSN, 2005: p. 1392-1320.

141. Motoyasu, G., et al., Continuously cast Cu-Al-Ni shape memory wires with a unidirectional morphology. Metallurgical and Materials Transactions A, 2001. **32**(3): p. 585-593.

142. Lee, J. and C. Wayman, Grain refinement of a Cu-Al-Ni shape memory alloy by Ti and Zr additions. Trans Jpn Inst Met, 1986. **27**(8): p. 584-591.

143. Yang, N., C. Laird, and D.P. Pope, The cyclic stress-strain response of polycrystalline, pseudoelastic Cu-14.5 wt pct Al-3 wt pct Ni alloy. Metallurgical Transactions A, 1977. **8**(6): p. 955-962.

144. Funakubo, H., Shape Memory Alloys. 1987: C R C Press LLC.

145. Husain, S. and P. Clapp, The intergranular embrittlement of Cu-AI-Ni β-phase alloys. Journal of materials science, 1987. **22**(7): p. 2351-2356.

146. Shimizu, K. and K. Otsuka, Optical and electron microscope observations of transformation and deformation characteristics in Cu-Al-Ni marmem alloys, in Shape Memory Effects in Alloys. 1975, Springer. p. 59-87.

147. Suezawa, M. and K. Sumino, Lattice distortion and the effective shear modulus along a coherent twin boundary. physica status solidi (a), 1976. **36**(1): p. 263-268.

148. Izadinia, M. and K. Dehghani, Structure and properties of nanostructured Cu-13.2Al-5.1Ni shape memory alloy produced by melt spinning. Transactions of Nonferrous Metals Society of China, 2011. **21**(9): p. 2037-2043.

149. Bhattacharya, K., Microstructure of Martensite: Why it Forms and how it Gives Rise to the Shape-memory Effect. 2003: OUP Oxford.

150. Churchill, C.B., J.A. Shaw, and M.A. Iadicola, Tips and tricks for characterizing shape memory alloy wire: Part 3-localization and propagation phenomena. Experimental Techniques, 2009. **33**(5): p. 70-78.

RESUME

Muhammad Riad Abd al-Amir al-Mahdi, he completed high school education in Alkindi School, after that, he started undergraduate program in babylon University Department of in material Engineer 2009. Then in 2021 he started assignment as a Research Assistant in babylon University Department of material Engineering. To complete M. Sc. education, he moved to Karabuk University: where he has been still working as a R. A. for.!